Inorganic Chemistry

Article

pubs.acs.org/IC

The Modulation of Jahn–Teller Coupling by Elastic and Binding Strain Perturbations—A Novel View on an Old Phenomenon and Examples from Solid-State Chemistry†

Dirk Reinen

Fachbereich Chemie der Philipps-Universität, D-35032 Marburg, Germany

Related Paper

ABSTRACT: Cations in 6-coordination with orbitally degenerate E_g ground states, such as Cu^{2+} and low-spin Co^{2+}, play an important role in coordination chemistry—in particular, in modern complex biochemistry. The stereochemistry and the binding properties within the basic polyhedra are the subject of pronounced modifications due to vibronic coupling in such cases, but may be also significantly influenced by what is usually called an imposed strain. The latter effect makes allowance for the general observation that the host sites into which the Jahn–Teller unstable centers are substituted are seldom of O_h symmetry and built from six equal ligands. Hence, the finally observed molecular and binding structure of the pseudo-octahedral complex is the result of the combined action of vibronic coupling and strain. The closer analysis of host-site strain effects demands to distinguish between elastic strain components, which modify the force constant of the vibronically active (here, ε_g) vibration, and binding strain perturbations, which take account of possibly present ligands with different binding properties. A symmetry-met semiempirical strain model on such a basis is presented and a corresponding formulation within the vibronic coupling formalism is given, on the molecular level. Well-established model examples of Cu^{2+} in octahedral fluoride coordination in various host solids, where a great variety of experimental results is available, are given. The derived parameters allow a detailed characterization of the structural and energy qualities of the Jahn–Teller centers, and might help to steer these properties in cases where synthesis strategies are needed. The proposed strain concept is more complex than that of Ham [F. S. Ham, *Electron Paramagnetic Resonance*; Plenum Press: New York, 1972; F. S. Ham, *Phys. Rev.* **1965**, *A138*, 1727]; the advantage is that it is directly tied to the structure and energy of the Jahn–Teller complex in focus, although more data (experimental and possibly computed) are needed in such a model.

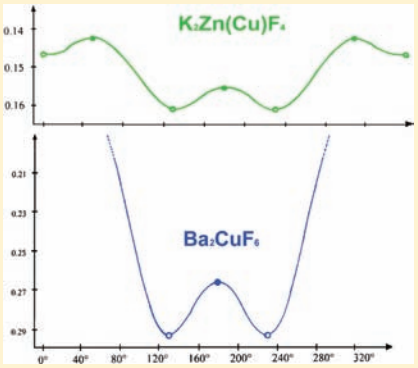

1. INTRODUCTION

If one studies the structural and energy aspects of vibronically unstable species in a solid matrix, one rarely encounters a situation where the host site possesses the highest possible symmetry. Thus, the lower-symmetry components of such a site add to the effects due to vibronic coupling in an often-complex manner. This interplay between the vibronic instability and the imposed energy and structural features of the host site, which are commonly termed "strain", is the subject of this study.

Strain effects, by the host lattice via its symmetry, composition, and structure, are of great significance in the chemical reality, if the stereochemistry and the energy modulation of doped Jahn–Teller (JT) guest centers in their specific local environment are investigated. In particular, the d^9-configured Cu^{2+} ion, whose ^2E_g ground state in O_h symmetry is the subject of strong $E_g \otimes \varepsilon_g$ vibronic interactions,[1] is rather thoroughly studied. Numerous fine investigations have been performed, with the aim of elucidating the shape and energy of the ground-state potential surface in detail. They will be appreciated and broadly discussed in the final section in relation to the then-available strain model, which is developed now.

The basic determinant, which considers the Jahn–Teller coupling of octahedrally coordinated Cu^{2+} in the ^2E_g ($t_{2g}^6e_g^3$) ground state, is of the form[2]

$A_{1g}(d_z^2)$	$B_{1g}(d_{x^2-y^2})$	(1)
$A_1\rho_\varepsilon\cos\phi - A_2\rho_\varepsilon^2\cos2\phi - E$	$-A_1\rho_\varepsilon\sin\phi + A_2\rho_\varepsilon^2\sin2\phi$	$= 0$
$-A_1\rho_\varepsilon\sin\phi + A_2\rho_\varepsilon^2\sin2\phi$	$-A_1\rho_\varepsilon\cos\phi + A_2\rho_\varepsilon^2\cos2\phi - E$	

It has the well-known solutions—after having added the totally symmetric restoring energy $^1/_2K_\varepsilon\rho_\varepsilon^2$—summarized in Appendix A. A_1 is the linear and A_2 is the second-order coupling parameter, which mainly comprises the $3d_{z^2}$–4s interaction (see Appendix A for details).[3] The latter stabilizes a B_{1g} ($e_g^4b_{2g}^2a_{1g}^2b_{1g}^1$)-ground state and a molecular D_{4h}^e-symmetry, in respect to the alternative $A_{1g}(b_{2g}^2e_g^4b_{1g}^2a_{1g}^1)$-state in D_{4h}^c (where the superscripts e and c represent elongated and compressed, respectively). K_ε is the force constant of the JT-active

Received: September 2, 2011
Published: March 14, 2012

 © 2012 American Chemical Society dx.doi.org/10.1021/ic202209c | *Inorg. Chem.* 2012, 51, 4458–4472

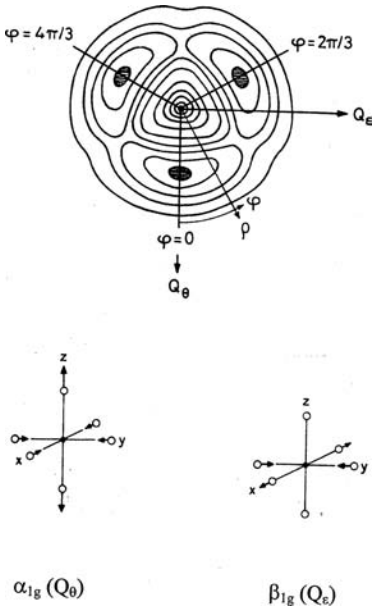

Figure 1. Ground-state potential surface due to $E_g \otimes \varepsilon_g$ vibronic coupling: The contour plot perpendicular to the energy axis ($Q_\theta = \rho_\varepsilon \cos \varphi$; $Q_\varepsilon = \rho_\varepsilon \sin \varphi$); the active vibrational mode (ε_g) components are depicted below.

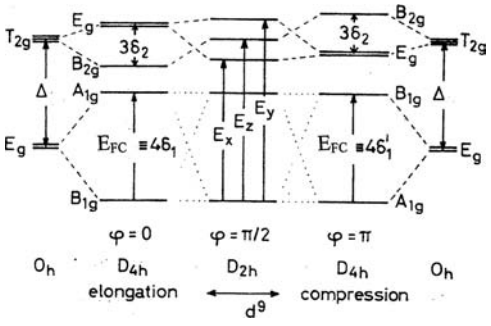

Figure 2. Schematic diagram of octahedral Cu^{2+} due to $E_g \otimes \varepsilon_g$ coupling (adopted from ref 11): The energy dependence on the angular parameter φ. The sequence of excited states in D_{2h} symmetry, with respect to the A_g ground state, is A_g, B_{1g}, B_{2g}, B_{3g}, and the octahedral ligand field strength Δ is (coarsely) defined according to the center-of-gravity rule, using the ground-state and excited-state splitting parameters δ_1 (δ_1') and δ_2, respectively.

ε_g vibration (see Figure 1); ρ_ε and φ are the radial parameter and the angular distortion, respectively. The latter specifies the location of the distortion along the D_{4h}–D_{2h} pathway, as depicted in Figure 1, which displays, in a contour plot, the warping of the ground-state potential energy surface by the nonlinear A_2 coupling constant. Figure 2 shows a sketch of the ^2E_g ground and $^2T_{2g}$ excited-state splittings in $D_{4h}{}^e$ and $D_{4h}{}^c$; here, the splittings in an intermediate D_{2h} symmetry also are shown. Appendix A summarizes the equations that characterize the molecular structures and energies of the CuL_6-octahedra in their host lattices solely as the result of vibronic coupling. In the subsequent section, the modification of these expressions will be considered, if host site strains are present.

Two model structures, which we will use in the following, are depicted in Figure 3. The constituting ZnF_6-octahedra in the K_2ZnF_4 and Ba_2ZnF_6 lattices form layers of corner-connected octahedra. While the two trans-ligands ||c are largely terminal (F_t)—only additionally weakly bonded to low-charged and

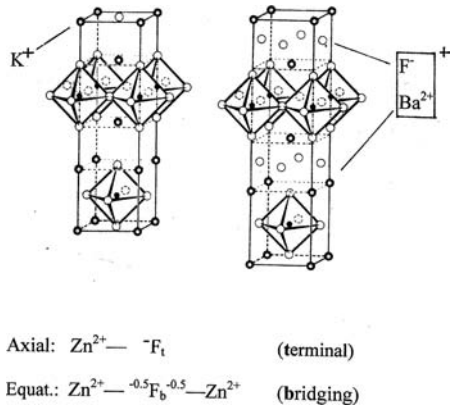

Figure 3. Structures of the host solids K_2ZnF_4 and Ba_2ZnF_6—with identical equatorial layers of corner-connected $Zn(F_t)_2(F_b)_{4/2}$ octahedra (Zn–F_t: ||z, approximately terminal, and Zn–F_b: $\perp z$), but differing interlayer lute (K^+ and BaF^+, respectively). The possible influence on the Zn–F binding properties, because of contrapolarization, is schematically sketched.

voluminous K^+ ions or $(BaF)^+$ groups—the four in-plane ligators (F_b) bridge two Zn^{2+} cations. The respective Zn^{2+}–$F_b{}^{-0.5}$ bonds might be different in character from the Zn^{2+}–$F_t{}^-$ bonds, because of the lower formal charge of the former ligand, which is introduced via the contrapolarizing power of the Zn^{2+} countercations within a $Zn(F_b\text{-}Zn)_4(F_t)_2$-cluster. A differing binding quality of $F_b{}^{-0.5}$ toward Zn^{2+}, as compared to $F_t{}^-$, is—in the perturbation model presented here—considered to originate from a *binding strain* ($A_1{}^s$), which supplements the first order coupling constant. The necessity to introduce such an increment is considered in detail in section 3.3. It is furthermore obvious, that, caused by the same structural features, the elastic properties of the ε_g vibrational mode are anisotropic in these lattices, favoring, for example, α_{1g}-type pathways leading to a tetragonal compression, rather than elongation (see Figure 1). The respective *elastic strain* component, which comes into play, if a $Zn(F_t)_6$ transforms to a trans-$Zn(F_b)_4(F_t)_2$ octahedron, is accounted for by the introduction of a force constant K_s, as a perturbation. A strain influence is indeed noticeably reflected by the structural properties of Ba_2ZnF_6; the constituting $Zn(F_t)_2(F_b)_4$-host octahedra, centered by the JT-stable Zn^{2+}-cation, are distinctly tetragonally compressed, with $\rho_\varepsilon = 0.10_5$ Å (see the definition of ρ_ε in eq A4),[4a] while they are nearly regular in K_2ZnF_4 ($\rho_\varepsilon \cong 0.00_5$ Å).[4b] The average bond length is $a_{av} = 2.025(5)$ Å in both cases.

If Ni^{2+}, with an orbital singlet $^3A_2$ ($t_{2g}{}^6e_g{}^2$) ground state, is substituted into the Zn^{2+} sites of the host solid, ligand field spectroscopy reveals discernible symmetry splittings of the octahedral transitions in the case of the Ba_2ZnF_6 lattice,[5] while the spectra of $K_2Zn_{1-x}Ni_xF_4$-mixed crystals are largely regular. The Δ values (7500 cm^{-1}) and B parameters (950 cm^{-1}) are identical in both cases. A lower-symmetry component (D_{4h} compression) is only revealed in the splitting of the lowest energy $^3A_{2g} \rightarrow {}^3T_{2g}$ ligand field band in the latter case,[6a] and is roughly estimated to be less than half of the magnitude of that in the $Ba_2Zn_{1-x}Ni_xF_6$ case. Here, exclusively, the *elastic (structural)* strain via K_s is brought to light. On the other hand, a binding strain may arise, if the bond strength of some anions toward the cationic center in a CuF_6 octahedron is modified; this is nicely documented by, for example, the d–d spectra of elpasolite-related (ordered ReO_3-type) solids $NiMe^{IV}F_6$ (Me^{IV} = Zr, Hf),[6b] which yield by 8% reduced ligand field and by ~3% enhanced Racah parameters, with respect to

dx.doi.org/10.1021/ic202209c | Inorg. Chem. 2012, 51, 4458–4472

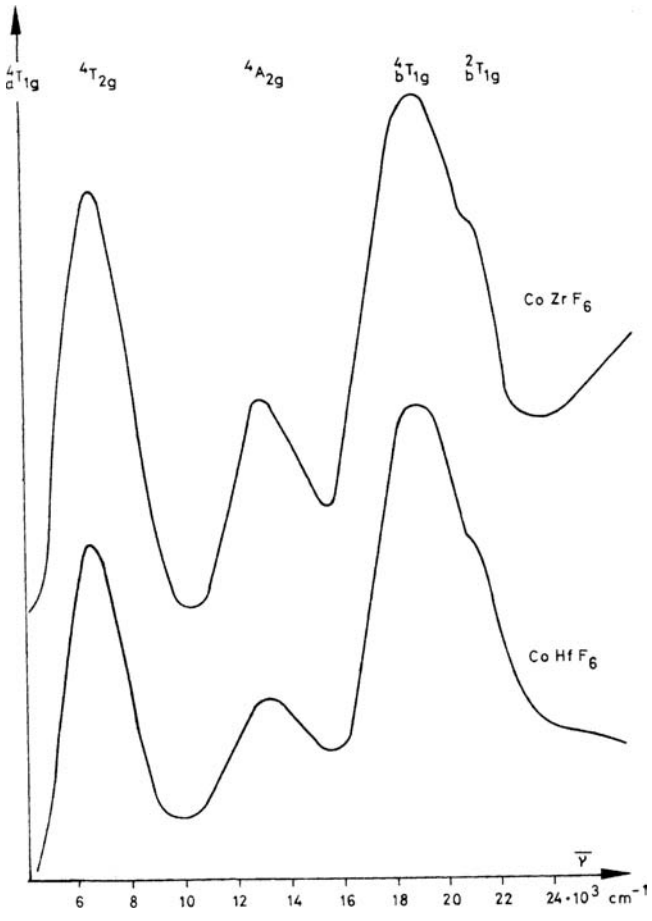

Figure 4. The d–d spectra of solids $Co^{II}Me^{IV}F_6$ with Me^{IV} = Zr, Hf.[6b] The three spin-allowed transitions occur at 6.7, 13.6, and 21.3 × 10^3 cm^{-1}.

Δ and *B* for K_2NiF_4 and Ba_2NiF_6: Δ = 6.9; *B* ≅ 0.98 × 10^3 cm^{-1} (see Figure 4). These data indicate a weakening and an ionicity increase of the Ni–F bond, which is due to the contrapolarization and the electron-withdrawing power of the Me^{IV} cations (see section 3.3). The d-d spectra of solids $CoMe^{IV}F_6$ (Me = Zr, Hf) in Figure 4 substantiate the rather good resolution, which characterizes the d–d spectra of this class of compounds.[6b] They mirror the same change, with a ligand field parameter Δ (7050 cm^{-1}), which is very near to that for Ni^{2+}, and a nephelauxetic ratio $\beta = B/B_0$ (*B* = 880 cm^{-1}), which is identical to that for Ni^{2+} (0.91).

Turning to the solids K_2CuF_4 and Ba_2CuF_6, Table 1 collects the well-established structural data for the constituting trans-$Cu(F_t)_2(F_b)_4$-octahedra, and furthermore lists the ground-state splitting E_{FC} (see Figure 2), as deduced from the ligand field spectra. Figure 5 displays the observed antiferrodistortive order of elongated octahedra in K_2CuF_4, which occurs in the $Cu(F_b)_{4/2}$ layers perpendicular to c, and further illustrates (as indicated by the arrows) that, in Ba_2CuF_6, the F_b ligands exhibit significant displacements away from linearity, with an angle ∠(Cu–F_b–Cu) of 154°. Here, we recall that the Me–F_t bond lengths shrink, when proceeding from the O_h (Me = Zn^{2+}) molecular symmetry to the D_{2h} (D_{4h}) molecular symmetry (Me = Cu^{2+}) in the overall displacement space. The designation "antiferrodistortive" characterizes an elastic cooperative order in which the long axes of neighboring D_{4h}-elongated octahedra are oriented perpendicular to each other.[11] The acentric movements of the bridging fluoride anions along the bond axes, which accompany the antiferrodistortive order, give rise to superstructure reflections. Their intensity is very weak in X-ray diffraction (XRD), because of the comparatively low number of electrons in the F^- ligand, but is pronounced in the case of neutron diffraction, because the scattering cross section of fluoride is rather large. Accordingly, the latter diffraction method yields more-reliable structural data—with distortion angles further away from 120° (240°) and also differing radial distortions (Table 1), in the cases considered here.

The schematic diagrams in Figure 6 (in accordance with the contour presentation in Figure 1) reflect the location of the two sublattices A and B, which constitute the antiferrodistortive

Table 1. Experimental and Calculated[a] Ligand Field Data (E_{FC} and E_{JT}),[b] and Structural Results (a_i, a_{av}, ρ_ε, φ)[c] for the Hexafluoro–Copper(II) Octahedra in Various Solids[d]

	a_i[e]	a_{av}/ρ_ε	φ	E_{FC}/E_{JT}	ref
Ba_2CuF_6	1.85 2.32_5 1.93_5	2.03_5 0.50_5[f]	130°[f] (230°)	≅9.7 *2.3*$_6$	7
Ba_2ZnF_6	*1.83*$_5$ *2.12*$_5$ *2.12*$_5$	(*2.03*$_5$) *0.34*$_0$	*180 ± 6°*	6.3 *1.5*$_9$	
K_2CuF_4[4b]	1.95 2.27_5 1.86_5	2.03 0.43_5[f]	109°[f] (251°)	8.3 *1.9*$_8$	8
K_2ZnF_4	*1.92*$_5$[g] *2.19*$_0$ *1.97*$_5$	(*2.03*) *0.27*$_8$	*130°* *(230°)*[g]	≅5.2 *1.3*$_0$	
$KCuF_3$	*1.98* *2.26* *1.86*	2.03_5 *0.41*$_4$[h]	*103°*[h] *(257°)*	≅8.1 *1.9*$_4$	9[h]
$KZnF_3$	*1.96* *2.18*$_5$ *1.96*	(*2.03*$_5$) *0.26*$_9$	120° (240°)	≅5.0[i] *1.2*$_6$	
$CuMe^{IV}F_6$	≅*1.96*$_5$ ≅*2.16* ≅*1.96*$_5$	(≅2.03) ≅*0.2*$_3$	120° (240°)	5.9 ≅*1.4*$_0$	10
$ZnMe^{IV}F_6$	~*1.98*$_5$ ~*2.12* ~*1.98*$_5$	(≅2.03) ~*0.1*$_6$	120° (240°)	~4.0[j] ~*0.9*$_7$	

[a] Calculated values given in italics are derived from the parameters in Table 3 (presented later in this work), utilizing the equations in Appendix B. [b] E_{FC} and E_{JT} data given in terms of × 10^3 cm^{-1}. [c] Data obtained from neutron diffraction; a_i, a_{av}, ρ_ε given in units of Å. [d] Citations refer to structural data. [e] In the sequence *i* = *z*, *x*, *y*. [f] X-ray diffraction (XRD) yields the following: ρ_ε^m ≅ 0.52 Å and φ_m ≅ 119° (241°) for Ba_2CuF_6;[4b] and $\rho_\varepsilon^m = 0.36_5$ Å and φ_m = 115° (245°) for K_2CuF_4.[4a] [g] Averaging according to a tetragonal compression occurs at the EPR time scale, with estimated bond lengths of *1.90 (3)* Å (2x), *2.09*$_5$ (*1.*$_5$) Å (4x). [h] The experimental data from XRD analysis are as follows: ρ_ε^m = 0.38 Å, φ_m = 109°, 251°, yielding: 1.96, 2.25, 1.89 Å for the a_i (*i* = *z*, *x*, *y*; $a_{av} = 2.03_5$ Å).[9] [i] Extrapolated from the reported value for the mixed crystal with *x* = 0.1 (0.66 eV) toward that for the doped solid.[17] [j] The reported energy is coarsely estimated from the d–d spectra (see Figure 12, presented later in this work) and via EPR (see text).

dx.doi.org/10.1021/ic202209c | *Inorg. Chem.* 2012, 51, 4458–4472

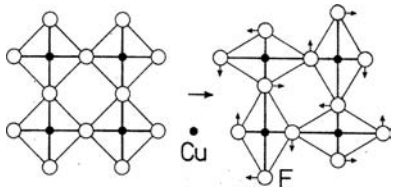

Figure 5. The antiferrodistortive order of elongated (with a D_{2h} distortion component) $Cu(F_t)_2(F_b)_{4/2}^{2-}$ octahedra in the solids K_2CuF_4 and Ba_2CuF_6 (adopted from ref 11). The view into the equatorial planes ($\perp F_t$) shows via small arrows the displacements, leading to nonlinear Cu−F_b−Cu bond sequences, as in the case of Ba_2CuF_6.

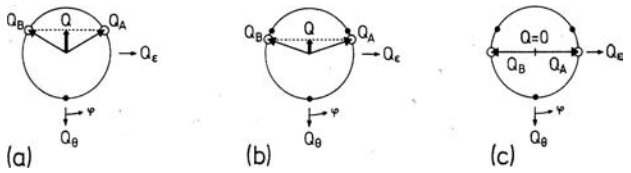

Figure 6. Schematic diagrams of the ground-state potential surface (adopted from ref 11), illustrating the angular locations of the two sublattices A and B, which establish an antiferrodistortive order according to $Q = -\rho^{af}$ (where ρ^{af} is the resulting radial lattice distortion). Constituting sublattices are located at (a) φ = 120° and 240°, (b) at 109° and 251° (K_2CuF_4), and (c) at 90° and 270° (vanishing lattice distortion).

order in the $\varphi-\rho_\varepsilon$ plane. In Figure 6a, the sublattices correspond to D_{4h}-elongated octahedra; in Figure 6b, they possess an orthorhombic distortion component. If the Cu^{2+} concentration in mixed crystals of $K_2Zn_{1-x}Cu_xF_4$ or $Ba_2Zn_{1-x}Cu_xF_6$ is successively enhanced, cooperative-elastic interactions between the trans-$Cu(F_t)_2(F_b)_4$-octahedra come into play.[5,8] Solely according to these, a cooperative order with sublattices at φ = 90° (270°), as shown in Figure 6c, should be stabilized, with $\Delta a_z = 0$ and $\Delta a_x = -\Delta a_y$ ($-\Delta a_x = \Delta a_y$) (see eq A6 in Appendix A). This is so because, here, the unit-cell dimensions remain unchanged, with only the F_b ligands moving acentrically away from their octahedral positions along the molecular directions: ···Cu-F_b−Cu−F_b-Cu··· (see Figure 5). Hence, if one compares the $Cu(F_t)_2(F_b)_4$ centers, as present in solids such as K_2CuF_4 and Ba_2CuF_6, with the same guest entities, which are only doped into K_2ZnF_4 and Ba_2ZnF_6, the force constant K_ε is significantly modified, because of the perburbation by a cooperative-elastic strain contribution K_{co}, which favors a D_{2h}-type order with φ = 90° (270°).

I have tried to substantiate in an experiment-supported molecular point of view—that, in the cases analyzed here, two elastic and one binding strain parameters are necessary, or at least are helpful, in addition to the classical Jahn−Teller coupling constants, if the structural and energy landscape of vibronically unstable species in an arbitrary host is studied and analyzed. In the following section, the respective semiempirical strain model is specified.

2. THE STRAIN CONCEPT

The trivial symmetry condition sine qua non for the concept is that only strain contributions are taken into account, which interfere with the vibronic coupling terms in the $O_h \rightarrow D_{4h}$−D_{2h} landscape (see Figure 1). Lower-symmetry distortion components of the host octahedron are expected to just add to the final distortion. In the considered host lattices, distortion components of the latter type are not present. The proposed local binding strain parameter A_1^s is analogous to the linear A_1 coupling term (see eq 1), but with an angular parameter φ, which is constant and equal to the strain angle φ_s (see the energy eq B1 in Appendix B). This choice is obvious and corresponds to the Cu−F bond anisotropy, as present in the host octahedron. As will be shown in the following section, the binding strain is vanishing, within very narrow error limits of <3%, in the first investigated class of solids (see sections 3.1 and 3.2), but shows up strongly, if solids $Zn(Cu)Me^{IV}F_6$ are considered (section 3.3).

Also, the choice and the evaluation of the noncubic elastic strain contributions must be symmetry-comformable, according to a cos 3φ angular dependence. In the relation

$$\cos 3\varphi = (2\cos 2\varphi - 1)\cos\varphi \tag{2}$$

the (cos φ)-angular increment correlates with the α_{1g} pathway of the JT-active ε_g vibration in the respective polyhedron distortion, while the (cos 2φ) function mirrors the influence of the β_{1g} vibrational component. The latter has orthorhombic symmetry and controls the angular motions in the ground-state potential energy trough away from 0°; 180°; it generates further equivalent extremum points at 120°, 240°; 60°, 300° (Figure 1), via the stabilization of angular positions at 90° and 270°. It is now straightforward to also define a local elastic strain component, which takes account of a host site distortion away from the angular positions at φ = 0°, 120°, and 240°, which are favored by vibronic forces. In the case of Ba_2ZnF_6, for example, the host site is D_{4h}-compressed, and, accordingly, the strain possesses α_{1g}-symmetry, yielding a cosφ-type elastic perturbation:

$$E_s^{(1)} = -\frac{1}{2}K_s\rho_\varepsilon^2\cos(\varphi - \varphi_s') \quad [\varphi_s' = 180° \Rightarrow \frac{1}{2}K_s\rho_\varepsilon^2\cos\varphi] \tag{3}$$

The sign is chosen such that it stabilizes a tetragonal compression and a d_z^2 ground state, with the minimum at $\varphi = \varphi_s'$. Both angular distortion parameters—the above (φ_s) and the one here (φ_s')—refer to the structural data, as revealed by neutron diffraction and XRD. If the constituting ligands are significantly different, with respect to their binding properties, irritations may arise, because the bond *strengths* are not necessarily strictly proportional to the bond *lengths* anymore. Accordingly, the interpretation of φ becomes tricky, and the final φ_m angle may differ—depending on whether the *binding strain*, which reflects the bond strength, or the *elastic strain*, which mirrors the structure, is inspected (see also the discussion of this matter in Appendix C). If the ligator atoms are identical (vide infra), with only small or even vanishing differences, with respect to their binding properties, the sketched concept is expected to work well within the given limitations.

The second elastic strain perturbation comprises the cooperative-elastic interactions between the CuF_6 octahedra in Ba_2CuF_6 and K_2CuF_4; it correlates with the (cos 2φ) angular term in eq2 and refers to a stabilization of strain angles φ_s'' at 90° and 270° (see Figure 6c and section 1):

$$E_s^{(2)} = -\frac{1}{2}K_{co}\rho_\varepsilon^2\cos 2(\varphi - \varphi_s'') \rightarrow \frac{1}{2}K_{co}\rho_\varepsilon^2\cos 2\varphi \tag{4}$$

K_{co} images a *cooperative phenomenon* via the projection on a single molecular CuF_6 species. Besides K_{co}, a further *totally*

dx.doi.org/10.1021/ic202209c | Inorg. Chem. 2012, 51, 4458−4472

symmetric cooperative-elastic strain component is expected and indeed found to be present, which modifies the local force constant K_ε'—valid for the Cu^{2+}-doped solids—toward K_ε; the latter refers to the bulk Cu^{2+} solids and mirrors the total of the local components and those cooperative strain components, which are totally symmetric.

Summing up the various binding and elastic strain perturbations as additional energy quantities, one can construct the strain-modified matrix from eq 1, with the help of which the final potential energy and structural equations in Appendix B are easily obtained. Expressions B1−B3 yield, by minimization, with respect to the radial and angular distortion parameters, eqs B4−B6, which define the experimentally accessible quantities $\rho_\varepsilon{}^{m}$ and φ_m (see Figure 6). The ground-state splitting at the absolute minimum, E_{FC} (= $4\delta_1$ or $4\delta_1'$ in $D_{4h}{}^{e}$ or $D_{4h}{}^{c}$, for example; see Figure 2), is specified in eq B7. The sketched model is semiempirical, in contrast to the rigorous approach of Ham.[12] However, it has the advantage that it is more diversified and bears direct relation to experimental quantities and chemical concepts, such as the ubiquitously present phenomena in the chemical reality: structure and bonding. It distinguishes between elastic and binding strain perturbations, with the result, that the former, via the radial distortion, may have an even more pronounced influence than the latter. A less-sophisticated strain approach along the same line is found elsewhere.[13]

3. THE APPLICATION

The ligand field parameter and the linear coupling constant are related to the angular-overlap parameters e_σ (and e_π) via the following expressions:

$$\Delta = 3e_\sigma - 4e_\pi \tag{5a}$$

$$A_1 = \left(\frac{\sqrt{3}}{2}\right)\left(\frac{de_\sigma}{da}\right) \tag{5b}$$

Although Δ—and, hence, e_σ (e_π is small, compared to the σ-antibonding energy)—reflects the Cu−F bond strength, the magnitude of A_1 is given by the gradient of e_σ, with respect to the bond length;[14] accordingly, the linear coupling measures the bond covalence, and increases with the bond ionicity, if e_σ remains approximately constant. The mutual correlation of Δ and A_1 in eqs 5 is, for example, for the JT cation Mn^{III}, nicely mirrored via the d−d spectra and the octahedron distortions in elpasolite-type solids $A_2A'Mn^{III}F_6$ (A and A′ are large alkaline cations), where the F^- ligands are largely terminal, in comparison to compounds $AMn^{III}F_4$. There, analogous to the stereochemical situation analyzed here, the bridging fluoride ligands in the equatorial plane of the constituting trans-$Me(F_t)_2(F_b)_4$ octahedra undergo a significant $F_b \rightarrow Mn^{III}$ charge transfer, because of a pronounced contrapolarization by the respective spacially opposite-located Mn^{III} cations within the $Mn^{III}-F_b-Mn^{III}$ bridges.[13] The electron transfer reduces the $Mn^{III}-F_b$ bond strength and, hence, the magnitude of Δ, if compared with the binding situation within a $Mn^{III}-F_t$ bond. On the other hand, the electronegativity of fluoride is enhanced by the deduction of charge from the ligand and generates increased values of the gradient of e_σ and, accordingly, of the linear coupling constant, as well as larger nephelauxetic ratios ($\beta = B/B_0$). Equation 5c connects the decrease in Δ and the respective increase δA_1 in a coarse empirical relation, derived for the previously mentioned class of Me^{III} compounds,[13] where the octahedrally coordinated Me^{III} are open-shell cations of the $3d^n$ series and f adopts values of ∼3:

$$\left\{\frac{|\delta\Delta|}{\Delta(F_t)}\right\}\cdot\left\{\frac{A_1(F_t)}{|\delta A_1|}\right\} = f \tag{5c}$$

Similarly, a decrease in Δ and, accordingly, an increase in A_1 are observed in $CuMe^{IV}F_6$ solids, where the Me^{IV} cations exert an even stronger contrapolarizing influence on the JT cation; this class of solids is treated in section 3.3. In the cases of the compounds K_2CuF_4, Ba_2CuF_6, $KCuF_3$, and the corresponding Cu^{2+}-doped Zn^{2+} hosts, however, a noticeable contrapolarizing influence of this type is not observed. In agreement with the corresponding demand for a vanishing $A_1{}^{s}$ parameter, the Δ values of the solids, analyzed in the following two subsections, are constant with Δ = 6.8 (2) × 10^3 cm^{-1} (see Table 2).

Table 2. Results from d−d Spectroscopy, Analyzing the Splittings of the Excited T_{2g} State (see Figure 2)

	symmetry	Δ^a (× 10^3 cm^{-1})	$3\delta_2$ (× 10^3 cm^{-1})^a	ref(s)
Ba_2CuF_6	D_{2h}	≅6.9	^{b}	5
Ba_2ZnF_6 (Cu^{2+})	$D_{4h}{}^{c}$	6.9	2.5	5
K_2CuF_4	D_{2h} (≅ $D_{4h}{}^{e}$)	7.0_5	2.7	15, 17
K_2ZnF_4 (Cu^{2+})	D_{2h}	≅6.8	^{b}	16
$KCuF_3$	D_{2h} (≅ $D_{4h}{}^{e}$)	≅6.8	2.6	11
$KZnF_3$ (Cu^{2+})	$D_{4h}{}^{e}$	6.6	1.7	17
$CuMe^{IV}F_6$	$D_{4h}{}^{e}$	6.1	1.8	6b, 18
$ZnMe^{IV}F_6$ (Cu^{2+})	$D_{4h}{}^{e}$	(6.1)	∼1.2^c	

^{a}As defined in Figure 2. $^b{}^2A_g \rightarrow {}^2B_{1g}$, $^2B_{2g}$, $^2B_{3g}$ transitions at 10.0, ∼12.0, 13.3 × 10^3 cm^{-1} for Ba_2CuF_6 and 8.2, 9.3, ∼10.7 × 10^3 cm^{-1}, for K_2ZnF_4 (Cu^{2+}), respectively, about halfway between $D_{4h}{}^{e}$ (φ = 120° and 240°) and $D_{4h}{}^{c}$ (φ = 180°). ^{c}Estimated via optical and electron paramagnetic resonance (EPR) spectroscopy (see text).

It should be mentioned and supplemented here, that the inter-relation between the contrapolarizing power of, in particular, highly charged and small cations on the one hand and the electronegativity and the donating power of an intervening ligand on the other hand has been thoroughly studied for oxygen as the anion,[19] and this has led to the useful concept of optical basicity.[20] The influence on the ligand field parameter Δ and the nephelauxetic ratio β—if divalent $3d^n$ cations are used as probes—can be rather distinct;[21] the resulting effects are diversified and not always easy to interpret.

If one assumes that (with the exception of K_s) the coupling parameters A_1 and A_2, as well as the force constants K_ε and K_{co}, are equal within narrow limits for Ba_2CuF_6, K_2CuF_4, and $KCuF_3$, nine equations of condition (eqs B4, B6, B7) are available. This approach is based on the structural finding that the octahedral $Cu(F_t)_2(F_b)_{4/2}{}^{2-}$ layers are identical in the two former solids, and are distinguished only if the interlayer lute is considered (see Figure 3). This gives rise to the further strain parameter K_s, which vanishes for the constituting $Cu(F_b)_6$ octahedra in $KCuF_3$. Following the structural results for the $Zn(F_t)_2(F_b)_4$ host octahedra (the ionic radii of Zn^{2+} and Cu^{2+} are almost identical), the elastic strain parameter K_s is very small in the K_2CuF_4 case ($\rho_\varepsilon \approx 0.00_5$ Å for K_2ZnF_4) and more significant for Ba_2CuF_6 ($\rho_\varepsilon \cong 0.10_5$ Å for Ba_2ZnF_6). After all, *six unknown coupling and elastic parameters are faced with a total of nine experimental quantities* (see Table 1). The common parameter set that is listed in Table 3 indeed fits the

dx.doi.org/10.1021/ic202209c | Inorg. Chem. 2012, 51, 4458−4472

Table 3. Vibronic Coupling Parameters and Force Constants for $Cu^{II}F_6$ Octahedra in Various Solid Matrices (Listed in Both eV and 10^3 cm^{-1} Energy Scales)[a]

Vibronic Coupling Parameters			
A_1[b]		A_1^s	A_2[c]
1.16 eV Å^{-1}		≅0 eV Å^{-1}	0.06_5 eV·Å^{-2}
9.36×10^3 cm^{-1} Å^{-1}		≅0 cm^{-1} Å^{-1}	$0.5_2 \times 10^3$·cm^{-1} Å^{-2}
Force Constants			
K_ε[d]	K'_ε[d]	K_s[e]	K_{co}[f]
3.2_5	4.4_5	1.1_5; 0.2_5	0.3_5 eV·Å^{-2}
$25._8$	$35._9$	9.2; 2.0	2.8×10^3·cm^{-1} Å^{-2}

[a]Note that 1 eV = 8.066×10^3 cm^{-1}. [b]Characterizing the $Cu(F_t)_2(F_b)_4$ octahedra in $Ba_2M^{II}F_6$ and $K_2M^{II}F_4$, as well as the $Cu(F_b)_6$ centers in $KM^{II}F_3$ (M^{II}: Cu^{2+}, Zn^{2+}). For the $M^{II}Me^{IV}F_6$-type solids with $Cu(F_b')_6$ centers, $A_1 \cong 1.5$ eV Å^{-1} (≅12×10^3 cm^{-1} Å^{-1}) has been used (see text). [c]A_2 is estimated to be enhanced to ≅0.3 eV Å^{-2} (≅2.4×10^3 cm^{-1} Å^{-2}) in the case of the $M^{II}Me^{IV}F_6$ compounds. [d]K_ε and K'_ε, for Ba_2CuF_6, K_2CuF_4, $KCuF_3$, and the Cu^{2+}-doped Zn^{2+} hosts, respectively. The magnitudes for the $Cu(F_b')_6$ octahedra in the solids $M^{II}Me^{IV}F_6$ are enhanced by a factor of ~2.2: $K_\varepsilon \cong 7._1$; $K'_\varepsilon \cong 9._9$ eV Å^{-2} (≅ 57; ≅ 80×10^3 cm^{-1} Å^{-2}). [e]The indicated values refer to $Ba_2M^{II}F_6$ and $K_2M^{II}F_4$, respectively. K_s is zero in the cases of $KM^{II}F_3$ and $M^{II}Me^{IV}F_6$. [f]Taking account of noncubic cooperative-elastic interactions between the CuF_6 octahedra in the solids Ba_2CuF_6, K_2CuF_4, and $KCuF_3$.

experimental data very well, within deviations of only a few percent. We have chosen observed structural data from neutron diffraction refinements as observables, because of the superior localization of F^-, in comparison to XRD; in agreement, EPR spectroscopy also suggests stereochemical data very close to those from neutron diffraction,[7] in the case of Ba_2CuF_6. Because only X-ray data are available for $KCuF_3$, the respective structural results (ρ_ε^m, φ_m) were considered to be less crucial in the adaption procedure. The reference octahedron, which defines A_1, A_2, and K_ε and controls the magnitudes of the elastic (and binding) strain parameters in Table 3, is the weighted average of $Cu(F_t)_6$ (1/3) and $Cu(F_b)_6$ (2/3).

3.1. The Solids K_2CuF_4, Ba_2CuF_6, and Cu^{2+}-Doped K_2ZnF_4 and Ba_2ZnF_6. Figure 7 shows the ground-state stabilization energy (E_{JT}) in dependence on φ (see eqs B5 and B4) for Ba_2CuF_6 and K_2CuF_4. The angular positions 0° and 180° correspond to D_{4h}-elongated and D_{4h}-compressed—in both cases parallel to the Cu−F_t bonds (molecular z-direction)—trans-$Cu(F_t)_2(F_b)_4$ octahedra (see Figure 3), with $d_{x^2-y^2}$ and d_{z^2} ground states, respectively; at these angles, the two sublattices become identical, constituting a ferrodistortive order (of tetragonally elongated and compressed octahedra, respectively). One recognizes that the latter steric arrangement (at $\varphi_m = 180°$) is energetically closer to the observed antiferrodistortive order of D_{2h}-elongated octahedra in Ba_2CuF_6 than in K_2CuF_4, because of the presence of a larger K_s value in the former case. However, both adiabatic energy curves indicate that an elongation of the hexafluoro-copper(II)-octahedra along the Cu−F_t bonds is the least-preferred choice, compared to expanding the Cu−F_b bonds instead. One further learns that the activation energy for destroying the cooperative JT order is, with ~450 and 225 cm^{-1}, respectively, larger in the case of K_2CuF_4 than for Ba_2CuF_6.

A challenging prospect might be to now apply the above considerations and formalisms to also the Cu^{2+}-doped Zn^{2+} host compounds, where only the ground-state splittings

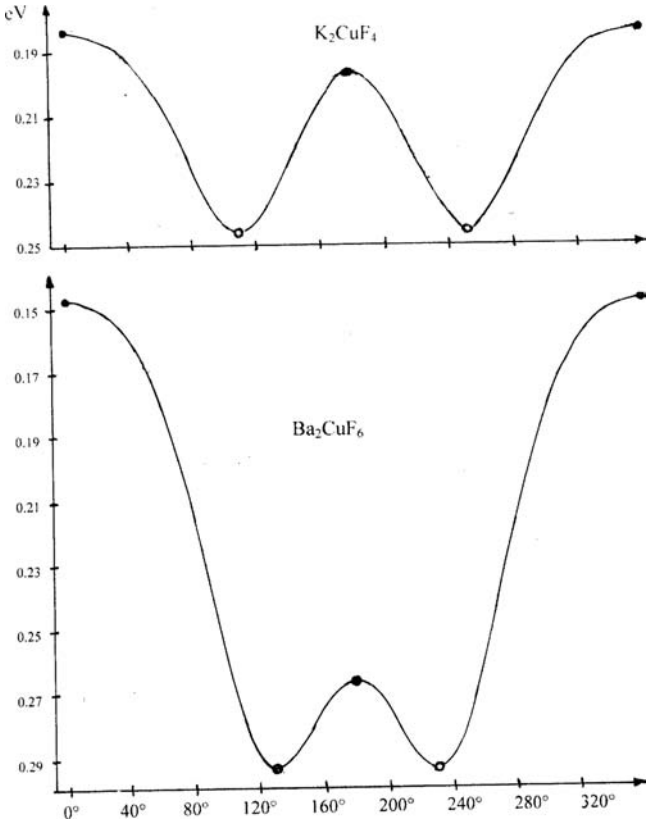

Figure 7. The ground-state potential energy curve: E_{JT} (eV) in dependence on the angular distortion φ, for Ba_2CuF_6 and K_2CuF_4—see eqs B5 and B4 with $\varphi_s = \varphi'_s = 180°$ and coupling parameters and force constants (K_ε, K_s, K_{co}) as listed in Table 3. The two sublattices at $\varphi_m = 130°$ and 230°, and 109° and 251°, respectively, constitute the antiferrodistortive order. The radial distortion varies between $\rho_\varepsilon^m = 0.50_7$ Å at the minimum positions and $\rho_\varepsilon^m = 0.25_4$ Å at the saddlepoint at 0° for the former solid and, less distinctly, between 0.42_5 Å and 0.31_6 Å in the K_2CuF_4 case.

(Table 1) are known as observables from d−d spectroscopy, in addition to significant results from electron paramagnetic resonance (EPR) spectroscopy. We can indeed nicely reproduce the experimental E_{FC} energies by using the same parameter set as that used for the bulk solids (trivially with $K_{co} = 0$), with the exception of K_ε. Inspecting the different steric and elastic situation of an octahedron $Cu(F_t)_2(F_b)_4$, embedded in Ba_2CuF_6 or K_2CuF_4 and in the respective Zn^{2+} host solids, we expect a force-constant K_ε' in the latter cases, which is larger than K_ε, which is found indeed (see Table 3). This enhancement is obviously caused by the disappearence of a cooperative strain contribution of *cubic symmetry*, which is part of the elastic interactions between the CuF_6 octahedra in the fully substituted solids (see the foregoing discussion). The absolute minima of the ground-state potential energy curves have considerably shifted toward 180°, particularly in the case of Cu^{2+}-doped Ba_2ZnF_6, because of the vanishing K_{co} contribution with its tendency to stabilize molecular structures with β_{1g} symmetry, at $\varphi = 90°$ or 270° (Figure 8).

In the case of Cu^{2+}-doped Ba_2ZnF_6, one finds, via eqB6c and with $K_{co} = 0$ and $K_s = 1.1_5$, $A_2 = 0.06_5$ eV Å^{-2} (Table 3), that only one broad minimum is present at $\varphi_m \cong 180° \pm 6°$, which suggests the stabilization of D_{4h}-compressed octahedra with a pure d_{z^2} ground state. This finding is in agreement with EPR spectroscopy, but also with d−d spectroscopy (see Appendix C

dx.doi.org/10.1021/ic202209c | Inorg. Chem. 2012, 51, 4458−4472

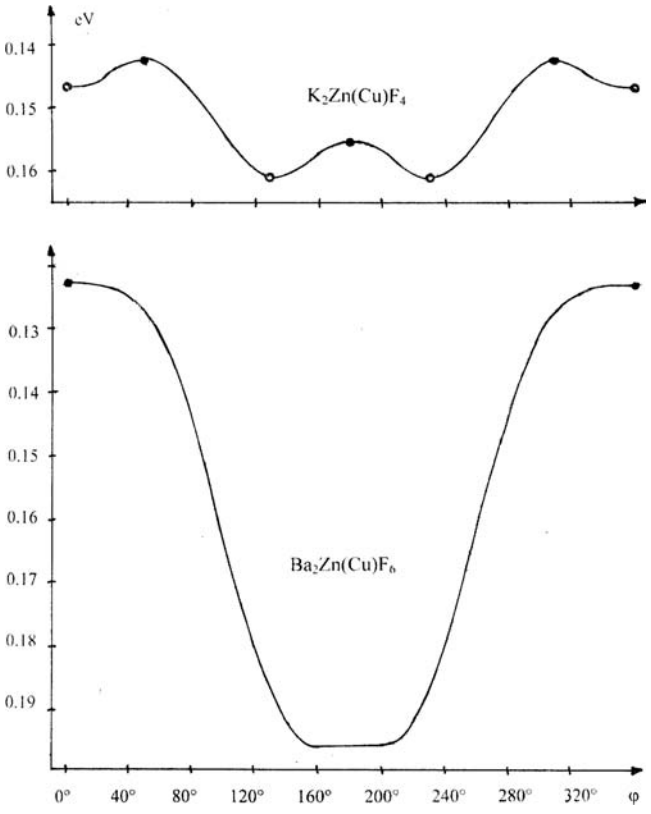

Figure 8. The ground-state potential surfaces: E_{JT} (eV) versus φ, for Cu^{2+}-doped Ba_2ZnF_6 and K_2ZnF_4—coupling parameters and force constants K'_ε, (K_s) as listed in Table 3 (K_{co} = 0). The energy scale is enlarged by a factor of 2, compared to Figure 7.

and below), where the time frame of excitation is shorter by several magnitudes of order.[5] In particular, the EPR-hyperfine splittings indicate a drastic reduction of the isotropic hyperfine constant from the value, characteristic of Cu^{2+} with a $d_{x^2-y^2}$ ground state ($\kappa_{3d} \cong 0.43$), to $\kappa \cong 0.10$.[22] This decrease is caused by the a_{1g} ($3d_{z^2}$) − a_{1g} (4s) interaction, which is symmetry-allowed for a d_{z^2} ground state in D_{4h}-compressed ligand fields, and corresponds to a 4s participation of ≅5%; the latter admixture reveals the finite probability of the unpaired electron to reside at the nucleus. After all, the potential energy curve, reflecting the parameter set in Table 3, can be considered to be realistic, also allowing one to report quantitatively more-reliable bond lengths in the trans-$Cu(F_t)_2(F_b)_4$ octahedra doped into Ba_2ZnF_6 (see Table 1) than previously observed.[5] The calculated radial distortion ρ_ε and the ground-state stabilization E_{JT} vary from 0.33_8 Å and 0.19_6 eV at φ_m = 180° to 0.21_2 Å and 0.12_3 eV at φ_m = 0° (see Figure 8). The interesting phenomena in respect to the transition from D_{4h}-compressed to D_{2h}-elongated octahedra in the mixed-crystal series $Ba_2Zn_{1-x}Cu_xF_6$ have been analyzed via, particularly, EPR spectroscopy by Friebel et al.[5] The EPR analysis is indeed the method of choice to distinguish, whether an observed (for instance, tetragonal compression) is *static* or only the *dynamic average* of two essentially elongated conformations (see the potential surface for Cu^{2+}-doped K_2ZnF_4 in Figure 8 as an illustrative example). The corresponding analytical expressions are given in Appendix C (see eqs C4).

The binding situation is more complex in the case of Cu^{2+}-doped K_2ZnF_4. The d−d spectra indicate orthorhombically distorted octahedra,[16] coarsely about midway between φ = 180° and 120°; in difference, the calculated minimum positions in the ground-state potential energy curve of Figure 8 (which rather reflect the structural data—see the discussion in Appendix C, Optical Spectroscopy) are shifted from the tetragonal positions by only ±10°, because of the presence of the finite, although small, K_s value. On the other hand, the EPR spectra are strictly tetragonal, but with the symmetry pattern of, along z, tetragonally compressed octahedra.[8,23] The latter observation is only contradictory at the first sight, but finds its explanation (as discussed before) in the comparatively much larger time frame of the EPR method, which averages the structural properties. The angular delocalization, estimated from the g-values, is considerable, with ∼180° ± 20° (see Appendix C, EPR Spectroscopy). In accordance, a significant admixture of $d_{x^2-y^2}$ to the d_{z^2} ground state is indicated, which should show up in the EPR-hyperfine structure. Indeed, the respective isotropic constant κ is found to be 0.27 and, hence, is intermediate between the values for a $d_{x^2-y^2}$ (≅0.43) and a pure d_{z^2} ground state (≅0.10; Ba_2ZnF_6 (Cu^{2+}));[24] it suggests an admixture of ≅2.5% 4s-character to the ground state, half in magnitude of the value for Cu^{2+}-doped Ba_2ZnF_6. The origin of the flat appearence of the adiabatic ground-state energy curve and of the shift of the absolute minima (from 109° (251°) in the case of $K_2Cu_2F_4$ toward φ > 120° (<240°)), is mainly the vanishing cooperative elastic strain due to K_{co}, but also the presence of the small, although significant elastic strain via K_s, which additionally lowers the energy barrier between the maximum at φ_m = 180° and the absolute minima noticeably (see $K_2Zn(Cu)F_4$ in Figure 8, in comparison with $KZn(Cu)F_3$ in Figure 10, presented later in this paper). The latter feature matches with the delocalization of the ground-state wave function within the EPR time frame, in contrast to optical spectroscopy, which reveals the instantaneous spacial situation. The radial distortion parameter varies between 0.24_6 Å at the two saddlepoints at φ_m = 50° (310°) and 0.27_8 Å at the absolute minima at φ_m = 130° (230°). The thermal excitation energy for an occupation of the minimum at φ_m = 0° from the lower minima is $\Delta E = E_{JT}$ (130°) − E_{JT} (50°) ≅ 150 cm^{-1}. One might argue, that the deviation of the octahedron distortion from D_{4h}[c] in Cu^{2+}-doped K_2ZnF_4 is the result of still-present, although weak, cooperative-elastic interactions that are due to cluster formation. I think that this argument does not hold, because the EPR analysis refers to experimental data, which are deduced for the $KZn_{1-x}Cu_xF_4$-mixed crystal series by extrapolation to x = 0.[8] On the other hand, the optical spectrum of Cu^{2+}-doped K_2ZnF_4-single crystals indicates a $Cu(F_t)_2(F_b)_4$-distortion symmetry about midway between D_{4h}[e] and D_{4h}[c], and hence far away from a tetragonal compression[16] (Appendix C, Optical Spectroscopy). After all, the vibronic landscape, mirrored by the potential energy curve of K_2ZnF_4 (Cu^{2+}), reflects the experimental data sufficiently well. We repeat, as the reliable outcome, that, in Ba_2ZnF_6, the CuF_6 octahedra are D_{4h}-compressed and possess a d_{z^2} ground state, while these octahedra in the K_2ZnF_4 host are of orthorhombic symmetry with a significant $d_{x^2-y^2}$ admixture of at least 10% to the d_{z^2} ground state. In the time frame of EPR, the molecular structure averages to a tetragonal compression also in the latter case (see Table 1). We note that the results for both Cu^{2+}-doped Ba_2ZnF_6 and K_2ZnF_4 are obtained by the adaption of only *one* new parameter, K'_ε, which reproduces *two* experimental E_{FC} energies; furthermore, the EPR evidence fully supports the deduced conclusions. While the $K_2Zn(Cu)F_4$ potential surface exhibits the full number of minima and saddlepoints, there is only

dx.doi.org/10.1021/ic202209c | *Inorg. Chem.* 2012, 51, 4458−4472

one (very broad) minimum and one saddlepoint in the case Cu^{2+}-doped Ba_2ZnF_6, because of the large K_s-force constant (eq B6).

The elastic properties of the solids considered thus far, within the proposed model, display a diversity according to the following properties:

- K_ε' is the local force constant of the octahedra Cu^{2+} centers, doped into the hosts.
- In the cases of Ba_2CuF_6 and K_2CuF_4, K_ε' is reduced toward K_ε, because of cooperative-elastic interactions between the Cu^{2+} octahedra; these interactions possess also a noncubic component, as outlined above, which gives rise to the force constant K_{co}. Because of its definition as the symmetry-equitable projection of cooperative-elastic forces onto the elastic properties of single molecular entities, it is not trivial to correlate K_{co} with the macroscopic force constants governing the cooperative JT effect in solids.[25]
- K_s (as well as A_1^s, which refers to the binding strain) mirrors the local bond length anisotropy in the host sites.
- The consistency of such a description is verified by the observation that the same force constants K_ε', K_ε, and K_{co} derived here can also be used in the case of the solids $KCuF_3$ and $KZn(Cu)F_3$, treated in the following section (K_s is vanishing, for obvious reasons).

3.2. The Perovskites $KCuF_3$ and Cu^{2+}-Doped $KZnF_3$.

The structure of $KCuF_3$ is derived from the cubic perovskite lattice and shows the same antiferrodistortive order of (approximately) tetragonally elongated octahedra as observed in Ba_2CuF_6 and K_2CuF_4 (see Figure 9). However, the F^- ions

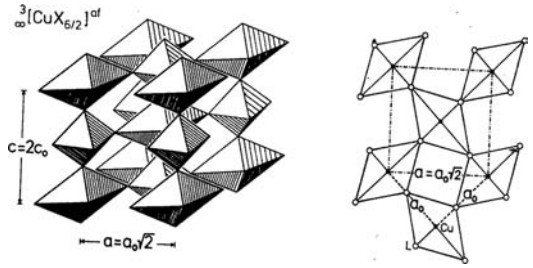

Figure 9. The antiferrodistortive order of elongated $Cu(F_b)_6$ octahedra in the perovskite lattice, observed for $KCuF_3$, and a view into the (001) plane; the K^+ positions, which turn the ReO_3 into the perovskite structure, are not indicated (adopted from ref 11).

in the lattice *c*-direction are equally bridging as in the equatorial planes, yielding $Cu(F_b)_6$ octahedra, which are homogeneous in the local elastic (and binding) properties. One can now deduce the structural parameters ρ_ε^m and φ_m at the absolute minima of the ground-state potential surface, and the ground-state splitting as well, using the same vibronic parameters as in the preceding cases (see Table 3) and when utilizing the three equations of condition (eqs B4, B6c, B7; with A_1^s, $K_s = 0$, and K_ε as for Ba_2CuF_6 and K_2CuF_6). The calculated data reproduce the experimental values within narrow limits. The deduced Cu−F_b bond lengths differ by about ±0.02 Å from those reported in the literature (see Table 1). There are numerous XRD studies, the results of which do not differ essentially from those of Okazaki and Suemune in 1961,[9] with respect to the bond-length data. However, different stacking orders ||c may occur, without influence on the local distortion of the $Cu(F_b)_6$ octahedra. As expected, the φ_m values, derived from the X-ray results (neutron diffraction data are not available), are nearer to $\varphi = 120°$ (240°) than those calculated via the model proposed here. After all, the proposed parameter set (see Table 3) can be considered to be trustworthy. The ground-state potential surface possesses two absolute minima at $\varphi_m = 103°$ and 257°, with $\rho_\varepsilon^m = 0.41_4$ Å and $E_{JT} = 0.24_0$ eV (see Figure 10).

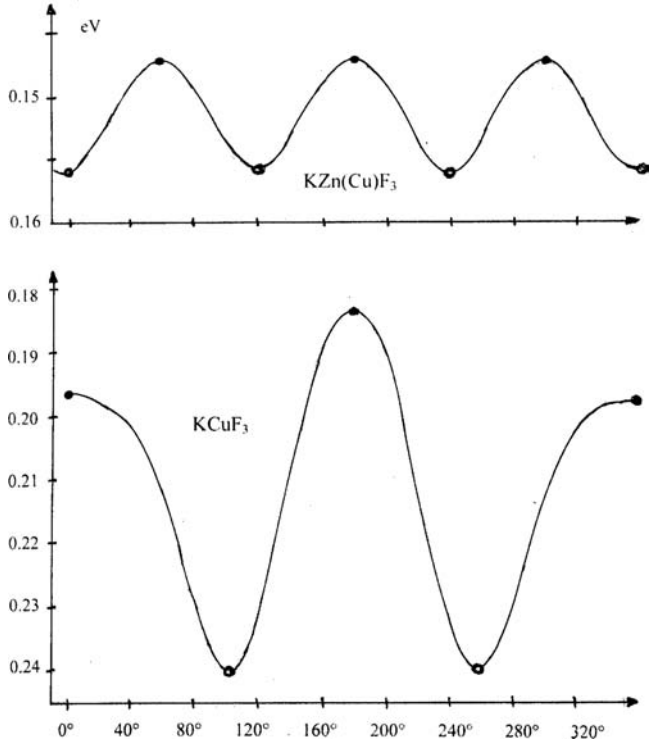

Figure 10. The ground-state potential surfaces: E_{JT} (eV) versus φ, for the $Cu(F_b)_6$ octahedra in $KCuF_3$ and $KZn(Cu)F_3$. The parameters used are $A_1 = 1.16$ eV Å^{-1}; $A_2 = 0.06_5$ eV Å^{-2}, as well as $K_\varepsilon = 3.2_5$, $K_{co} = 0.3_5$, and $K_\varepsilon' = 4.4_5$ eV Å^{-2}, respectively. The energy scale is enlarged by a factor of 2 in the former and 4 in the latter case, in comparison with Figure 7.

The saddlepoint at 180° ($E_{JT} = 0.18_3$ eV; $\rho_\varepsilon^m = 0.31_5$Å) is higher in energy than that at 0° ($E_{JT} = 0.19_7$ eV; $\rho_\varepsilon^m = 0.33_9$ Å), because of the K_{co} elastic contribution, which drives φ_m toward angular positions near to 90° (270°). The antiferrodistortive order with sublattices at $\varphi = 103°$ and 257° is stabilized, with respect to the ferrodistortive order at $\varphi = 0°$ (octahedra-elongated ||z) by 350 cm^{-1} (see Figure 10).

The ground-state splitting for $Cu(F_b)_6$ octahedra, doped into the $KZnF_3$ host, as deduced from reported optical spectra (Table 1), perfectly matches with the calculated E_{FC} transition energy—utilizing A_1^s, K_s, $K_{co} = 0$, and $K_\varepsilon' = 4.4_5$ eV Å^{-2}; the radial distortion parameter is derived to be $\rho_\varepsilon^m = 0.26_9$ Å. The potential energy curve shows three equivalent minima, instead of the two in the case of $KCuF_3$, and of only one for $Ba_2Zn(Cu)F_6$ (see Figure 8), in agreement with optical single-crystal studies, which unambiguously show that these centers are strictly tetragonal, according to D_{4h}^e (see Table 2).[16] The energy difference between these minima and the three saddlepoints at 60°, 180°, and 300° (at $\rho_\varepsilon^m = 0.25_3$ Å and $E_{JT} = 0.14_7$ eV) is given as

$$\Delta E \cong 2A_2(A_1/K_\varepsilon')^2 \qquad (6)$$

dx.doi.org/10.1021/ic202209c | Inorg. Chem. 2012, 51, 4458−4472

and has the magnitude of ≅70 cm^{-1}. The low energy barrier induces thermal averaging, in the D_{4h}^{e}-type EPR-spectrum already at temperatures above ∼20 K.[16] The Cu−F_b spacings in the tetragonally elongated octahedra, derived from ρ_{ε}^{m}, are listed in Table 1.

3.3. Solids $CuMe^{IV}F_6$ with Ordered ReO_3-Derivative Structures. It seemed worthwhile to experience whether one can also deduce meaningful structural and energy data for solids $CuMe^{IV}F_6$ (where Me^{IV} = Zr, Hf, Sn, Pb); here, strongly contrapolarizing Me^{IV} cations significantly affect the strength and quality of the Cu−F bond in trans-position: Cu^{2+}−F_b'−Me^{IV}. The mentioned compounds crystallize in the ordered ReO_3 structure or mostly in the hexagonal $LiSbF_6$ lattice, which is the ordered variant of the VF_3 structure; however, these solids also occur in the respective lower-symmetry Jahn−Teller descendants of these types.[26] The $LiSbF_6$ structure is a collapsed version of higher density (Figure 11, top right), with respect to the open ReO_3 lattice, with 12-coordinate holes in the cubic array (Figure 11, top left). The respective trigonal distortion occurs along a [111]-axis of the cubic ReO_3 lattice and corresponds to a rather small elongation along this direction; although it generates a molecular strain, acting along a 3-fold axis of the $Cu(F_b')_6$ octahedra, it does not interfere with the $E_g \otimes \varepsilon_g$ vibronic coupling in first order. Whether a solid adopts the hexagonal $LiSbF_6$ or the cubic ordered ReO_3 structure, or the respective lower-symmetry Jahn−Teller descendants (monoclinic and tetragonal, respectively), depends on the radius of the Me^{IV} ion, as well as on the "soft" or "hard" nature of the Me^{IV} cations, and (trivially) on the temperature also. While the solids with the d^{10}-configured Sn^{IV} and Pb^{IV} cations adopt the hexagonal $LiSbF_6$ structure at 293 K, Hf^{IV} and Zr^{IV} induce the following phase transitions, when exceeding the given transition temperatures:[26]

$CuHfF_6$	298 K	($LiSbF_6$-structure:	435 K	(hexag. $LiSbF_6$ →
$CuZrF_6$	353 K	monoclinic → hexag.)	383 K	ordered cubic ReO_3)

(7)

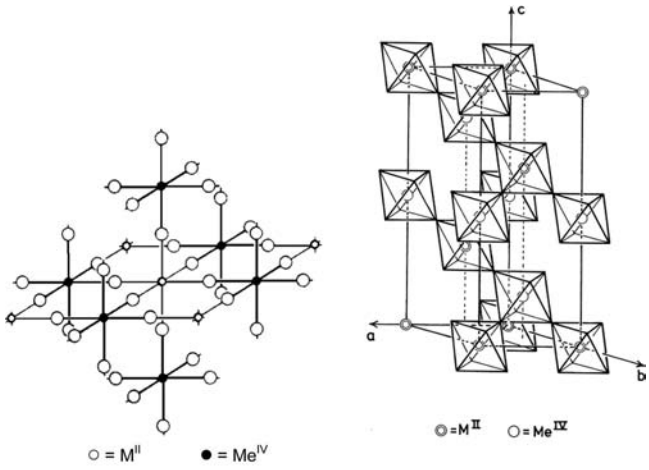

Figure 11. The ordered ReO_3 structure (top left) and the $LiSbF_6$ structure (top right, adopted from ref 27a) of solids $M^{II}Me^{IV}F_6$. The bottom sketch depicts the possible deviations of the F^- ligands from the ideal positions in the former, JT-modified lattice (adopted from ref 18, as sketched for $Cr^{II}ZrF_6$ at 298 K).

In the case of the corresponding Cr^{II} solids, where the $3d^4$ cation possesses an E_g ground state, as Cu^{2+} does, the JT-modified ordered ReO_3 structure with tetragonal symmetry also can be observed. Finally, one should notice that the two non-JT-phases do not only appear if the local JT-distortion becomes dynamic, but also if the long-range order between the $Cu(F_b')_6$ octahedra in the lattice breaks down. This is, for example, the case for $CuPbF_6$ at 298 K. After all, we meet a rich structural manifold in this class of compounds with JT-unstable cations, which makes it worthwhile to analyze the ground-state properties in greater detail. Though X-ray[27a] and neutron-diffraction[27b] analyses yielded reliable structural data for both types of lattices in the case of non-JT cations on the M^{II}-position, this is not so if Cu^{2+} and Cr^{2+} occur on that site. Here, because of the complexity of the spacial arrangements, which govern the local and cooperative lattice forces, only coarse structural data are available.[10] We are left with the following EPR- and d-d spectral results:

The ground-state splitting for the $Cu(F_b')_6$ octahedra is ≅5900 cm^{-1} (see Figure 12 and Table 1). The EPR spectra indicate a *strictly tetragonal* D_{4h}^{e}-symmetry with $g_{\parallel} = 2.60_5$, $g_{\perp} = 2.11_7$ for the single octahedra ($CuPbF_6$ at 293 K).[18] The latter are elastically coupled in an (frequently short-range, as in the cases of $CuPbF_6$ and $CuSnF_6$) antiferrodistortive order. There is, via exchange-coupling, EPR-spectral evidence that the distorted $Cu(F_b')_6$ octahedra in $CuZrF_6$ are long-range-ordered below 353 K, and undergo a thermal bond-length equilibration above this temperature (see eq 7). The order is spacially disturbed, however, because of Cu^{II}−F_b'−Me^{IV} angles, which may deviate from 180° by up to 40°. Nonlinearity of this type can also occur in the ReO_3 lattice (see Figure 11, bottom). Accordingly, the long and short Cu^{II}−F_b' bond directions of neighboring $Cu(F_b)_6$ octahedra are not aligned strictly perpendicular toward each other.

With solely this information at hand (only approximate structural data are available; see Table 1), one can nevertheless roughly estimate the linear coupling constant $A_1(F_b')$ via the approximate relation in eq 5c, yielding (with $\Delta(F_b) = 6.8$, $\Delta(F_b') = 6.1 \times 10^3$ cm^{-1} and $A_1(F_b) = 1.16$ eV $Å^{-1}$; see Tables 2 and 3), ≈ 1.5 eV $Å^{-1}$. With the further choice of $A_2 \approx 0.3$ eV $Å^{-2}$, as set forth below, we deduce a radial distortion parameter $\rho_{\varepsilon}^{m} \approx 0.2_3$ $Å^{-2}$ from eq B7. Besides K_s, K_{co} is also vanishing, because significant noncubic cooperative-elastic strain contributions, which would destroy the local D_{4h}^{e}-symmetry, are not present. A force constant of $K_{\varepsilon} \approx 7._1$ eV $Å^{-2}$ is calculated from eq B4, which more than doubles, with respect to the value for the previously considered solids. This must be attributed to the rigidity of the $Me^{IV}(F_b')_6$ octahedra, because these hard spacial structures act as effective ligands, which separate the Cu^{2+}

dx.doi.org/10.1021/ic202209c | Inorg. Chem. 2012, 51, 4458−4472

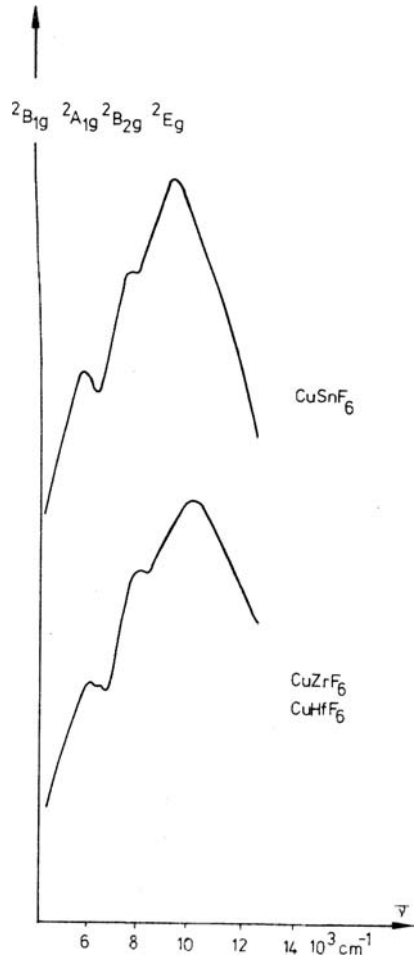

Figure 12. The d–d spectra of various $CuMe^{IV}F_6$ solids;[6b] band positions are listed in Tables 1 and 2.

cations in the lattice. The suggested parameter set (Table 3) generates a "normal" type of ground-state potential surface, analogous to that of Cu^{2+}-doped $KZnF_3$ (see Figure 10), but with a rather large energy barrier of ≅215 cm^{-1} between the three minima (see eq 6). Thus, the chosen A_2 parameter indicates a transition temperature of ≅310 K for the static-to-dynamic conversion (100 K ≈ 70 cm^{-1})—in fair agreement with the EPR and, in particular, the X-ray-Guinier data, which place the phase transitions in the suggested temperature-region (see the data collection in eq 7). The pronounced increase of A_2, compared to the value for the previously considered solids, is most certainly the distinctly enhanced ionicity of the Cu–F-bond, as may be deduced from the AOM expression[2] for this parameter:

$$A_2 \cong \frac{3}{4e_{ds}}\left(\frac{de_{ds}}{da}\right)^2 \qquad (8)$$

e_{ds}, with respect to the previously considered solids, mirrors the reduced $3d_z^2$–4s separation energy and should undergo an alteration, similar to e_σ. Having this in mind, A_2 is expected to increase by a considerably higher extent than A_1, as anticipated, because the derivative of e_{ds} appears quadratic in eq8, and, beyond that, as a divisor in this equation. Despite the distinct change in the Cu–F-bond character, when proceeding from the $F_{b,t}$ ligands to the F_b' ligands, the bond lengths remain almost unchanged;[26,27] this phenomenon was discussed already (see Appendix C, Optical Spectroscopy).

With the spectroscopic data from Figure 12, the orbital contributions to the g-tensor components are reproduced with $k_\parallel \cong k_\perp \cong 0.88_5$. The latter coefficient is distinctly enhanced in respect to those for Ba_2CuF_6, K_2CuF_4, and $KCuF_3$ ($k \cong 0.84$), which is an anticipated result, when recalling the similarly larger Racah parameter B in the case of the corresponding Ni^{2+} or Co^{2+} compounds. The excited-state splitting of 0.22 eV (see Table 2 and Figure 12) yields, via eqC1, a $T_{2g} \otimes \varepsilon_g$ coupling constant $V_\varepsilon \approx 0.6_5$ eV Å^{-1}, when using ρ_ε^m from Table 1; it is less enhanced than A_1 (≈ 1.5 eV Å^{-1}), with respect to the values for the previously considered solids (~0.5_6 and ~1.16 eV Å^{-1})—suggesting that the binding is basically of a σ-nature.

The experimental evidence in the case of the Cu^{2+}-doped compounds is meager. However, the experimental g-values ($g_\parallel \cong 2.66$; $g_\perp \cong 2.13$), when using the just-derived k-value, allow one to estimate the ligand field energies for the ($^2B_{1g} \rightarrow {}^2B_{2g}$)- and ($^2B_{1g} \rightarrow {}^2E_g$) transitions via eq C3c; these correspond reasonably well with only partly resolved d–d spectra. The E_{FC} ground-state splitting can be approximately derived, if one utilizes the Δ-value for the fully substituted solid (see Tables 1 and 2, as well as Figure 2). With the coarse information from the d–d spectra of the mixed-crystal series $Zn_{1-x}Cu_xZrF_6$[6b] in addition a seemingly consistent description is feasible, if a larger force constant K_ε' than that for the bulk solid is adopted (see Table 3). The energy barrier in the ground-state potential surface between the minima at 0°, 120°, 240° via the saddlepoints at 60°, 180°, 300° is ~109 cm^{-1} and roughly matches with the observation that an anisotropic EPR spectrum can only be observed at temperatures of <130 K.

The listed approximate parameter set for this class of solids (Table 3), together with the derived Δ-parameter (Table 2) and in comparison with the corresponding value for the previously analyzed compounds, allows a few significant statements:

- The $Me^{IV}(F_b')_6$ octahedra, which separate the Cu^{2+} ions in the lattice, are very rigid entities. They enhance the frequency of the JT-active e_g-vibration in a pronounced way (considerably larger K_ε, K_ε' force constants) and, furthermore, impede a long-range cooperative order between the D_{4h}-elongated octahedra ($K_{co} \cong 0$); however, the (negative) cubic contribution to the force constant ($K_\varepsilon - K_\varepsilon'$) remains significant.
- As the consequence of the increased ionicity of the Cu–F_b', with respect to the Cu–F_t– (and Cu–F_b) bonds, the linear coupling constant A_1 is significantly enhanced (by ~30%); nevertheless, the local Jahn–Teller distortion remains rather small, because of the also much-larger force constant (see eqB4). On the other hand, the ground-state splitting is still considerable; it is caused by the proportionality to A_1^2 (eq B7). The distinct increase of A_1 (Table 3) indicates that A_1^s is expected to adopt rather large values, if the F_t ligands in the Cu–F_t bonds would be partly substituted by F_b'–Me groupings with high-valency Me cations.
- The higher-order coupling constant A_2, which mirrors predominantly the $3d_z^2$–4s interaction, in the case of Cu^{2+} – is dramatically enhanced, if the bond ionicity increases.

dx.doi.org/10.1021/ic202209c | Inorg. Chem. 2012, 51, 4458–4472

4. PREVIOUS STUDIES AND DISCUSSION

In the early 1970s, there was extensive discussion about the spacial flexibility of octahedral Cu^{2+} due to vibronic $E \otimes \varepsilon$-coupling.[1,28] In the case of a linear interaction exclusively, the ground-state potential surface possesses a sombrero-shaped appearance, with a ringlike minimum without wharping (see Figure 1 and eqs A3 and A5 with $A_2 = 0$); hence, already small external disturbances are expected to stabilize any D_{4h} or D_{2h} distortion of the octahedron, in accordance with the symmetry conditions. This property initiated the plasticity concept by Gazo et al.[28,29] However, it was soon realized and confirmed by experiment that significant higher-order coupling is present, which preferentially stabilizes a tetragonal elongation. (See the remarks with respect to A_2 in Appendix A). Friebel could demonstrate, via EPR spectroscopy on Cu^{2+}-doped Ba_2ZnF_6,[5] that it is also possible to generate a tetragonal compression and, hence, a $A_1(d_z^2)$ ground state, if a strain from the lattice is applied, which opposes and overcompensates the vibronic tendency. More than a decade later, it was shown, via the analysis of the EPR-hyperfine structure of the same solid,[22] that a significant symmetry-induced admixture of A_1 (4s) to the A_1 ($3d_z^2$) ground state occurs (vide supra). This finding confirmed that it is indeed the $3d_z^2$–4s interaction that mainly determines the magnitude of the higher-order coupling constant A_2; it lowers the B_1 ($3d_{x^2-y^2}$), with respect to the $A_1(3d_{z^2})$ state and, accordingly, stabilizes the tetragonal elongation.[3] Sticking to fluoride as the ligand, the CuF_6 octahedra in $KCuAlF_6$ are further interesting examples of a tetragonal compression. The spectroscopic, structural, and magnetic analysis by Hitchman et al. revealed a considerable radial distortion with $\rho_\varepsilon^c = 0.28_5$ Å, induced by a significant lattice-induced strain, which is seen in the corresponding diamagnetic Zn^{2+}-host ($\rho_\varepsilon^c = 0.15_5$ Å).[30]

A detailed treatment to interpret—in particular, the energy properties of fluxional copper(II) complexes—has been developed by Riley et al.[31] (the RHW model). It uses the d–d spectra, the *g*-values from EPR spectroscopy, and the copper–ligand bond lengths from X-ray or neutron diffraction, as well as the thermal ellipsoid parameters, if available, and, more recently, also results from XAFS (all data sets are dependent on temperature) as experimental input parameters for the construction of the adiabatic ground-state potential energy curve.[32] Many informative and thorough interpretations, in terms of chemical bonding, resulted from this approach. However, the frequently adopted strain parameter *S*, as introduced by Ham,[12] remains a purely formal quantity, without the quality to serve as a source of information, with respect to the copper–ligand interaction. In contrast, in this contribution, the strain is defined in direct relation to the binding and the elastic properties within the parent octahedron of the host lattice, which may have advantages for understanding the phenomena involved, in terms of the nature of the chemical bond, which is a subject of interest not only for the experimental chemist.

As one interesting result, one learns that it is the presence of a local elastic strain (K_s) that transforms the trans-$Cu(F_t)_2(F_b)_4$ octahedra in Cu^{2+}-doped Ba_2ZnF_6 into D_{4h}-species, which are tetragonally compressed and accordingly possess a pure d_{z^2} ground state. In Cu^{2+}-doped K_2ZnF_4, on the other hand, the elastic strain is much smaller and only has the capacity to shift the distortion symmetry from D_{4h}^e at 120° (240°) to angular D_{2h} positions, which are almost intermediate between the latter and the tetragonal compression at 180°. Accordingly, a very significant percentage of $d_{x^2-y^2}$ is admixed to the d_{z^2} ground state. Here, it is interesting to note that, in oxidic solids of the K_2NiF_4 type and of a constitution such as La_2NiO_4, an external strain from the second-sphere coordination is present, which, because of the contrapolarization by the high-charged La^{III} cations toward the axial oxygen ligands, leads (opposite to the situation in K_2ZnF_4) to a very pronounced tetragonal elongation ($\|c$) of the NiO_6 octahedra, with $\rho_\varepsilon \cong 0.39$ Å ($a \cong 2.05$ Å).[33a] If Cu^{2+} substitutes Ni^{2+}, the distortion is strongly enhanced ($\rho_\varepsilon \cong 0.64$ Å; $a \cong 2.09$ Å).[33b] According to this finding, a very significant external strain is present, which is presumably largely of elastic origin (K_s), but it should have a distinct binding component (A_1^s) as well. Unfortunately, in these cases, the experimental data are scarce,[34] and a meaningful quantitative analysis, such as that for the fluorides, is not possible, because of overparameterization. This is also unfortunate, because of the role that La_2CuO_4 plays as a basic compound for the generation of high-temperature superconductivity.[35] From the viewpoint of solid-state chemistry, the near-to-square-planar coordination of Cu^{2+} in the latter compound favors the (partial) presence of Cu^{III} in the superconductors, because the (required) low-spin-configuration of the d^8 cation can only be enforced in such an extremely distorted site.[36] Confirming the latter statement, in the solid $La_2Li_{1/2}Cu^{III}{}_{1/2}O_4$ with an ordered distribution of Li^+ and Cu^{III} over the (pseudo-) octahedral sites, the well-defined local copper(III) centers are only very weakly bonded to their axial oxygen ligator atoms ($\rho_\varepsilon \approx 0.78$ Å).[37]

It is challenging to compare some outcomes of this contribution with the interesting recent results of Aramburu et al. from cluster calculations on $K_2Mg(Cu)F_4$—via DFT, with additional consideration of the Madelung potential energy contributions from the remaining frame of the K_2MgF_4 host lattice.[38] The authors report that the Cu^{2+}-octahedra are found to be tetragonally compressed. The magnitudes of the average bond length, the radial distortion parameter, and the Jahn–Teller energy, derived from the DFT LDA-type computations, are rather diverging for a 21-atom and a 37-atom cluster section of the lattice, respectively:

$$a_{av} = 2.03_3; \quad 1.99_5 \text{ Å}$$

$$\rho_\varepsilon{}^c = 0.20_0; \quad 0.11_5 \text{ Å}$$

$$E_{JT} \cong 0.30_4; \quad 0.08_6 \text{ eV}$$

The agreement with the data in Table 1 is remarkable only on a coarser scale. The radial distortion is clearly underestimated, and only the averaged Jahn–Teller energy is close to the value obtained by the experiment-based strain model presented here. Also, the considerable orthorhombic deviation of the local Cu^{2+} octahedra from $D_{4h}{}^c$ is obviously not reproduced. Theoretical and computational chemistry have become rather successful in recent years in mimicking the structures and energies of molecular systems, at least in the case of less-complex compounds, where even predictions of so far unknown properties could be made.[39] This is different, in particular in the case of solid-state systems with extended lattices, where the results from calculations still lack precision. The severe problem here is that the environment extends to infinity and, accordingly, any exact treatment must take the lattice periodicity and the involved space group symmetry into account. Not too many studies in transition-metal solid-state chemistry follow this line.[40] It seems that semiempirical

dx.doi.org/10.1021/ic202209c | Inorg. Chem. 2012, 51, 4458–4472

approaches in close inter-relation with the experiment, such as the one worked out here, are still qualified in the case of polyhedra, embedded into extended solids. Such models, although not fully rigorous in the demand of theory, can be advantageous for experimentalists, because they supply information, which can be directly translated into spacial and energy properties of the chemical bond. I recall here, for instance, the fine work of C. K. Jorgensen, who has created an experiment-based sight of ligand field theory, which is still of immediate interest.[20,41]

APPENDIX A

The $E_g \otimes \varepsilon_g$ Coupling Equations

The energy determinant described by eq 1 yields

$$E_{+/-} = \pm\left\{A_1^{\,2} + 2A_1A_2\rho_\varepsilon\cos 3\varphi + A_2^{\,2}\rho_\varepsilon^{\,2}\right\}^{1/2}\rho_\varepsilon + \frac{1}{2}K_\varepsilon\rho_\varepsilon^{\,2} \quad (A1)$$

and, for small values of $A_2^{\,2}\rho_\varepsilon^{\,2}$, with respect to $A_1^{\,2}$:

$$E_{+/-} = \pm(A_1 + A_2\rho_\varepsilon\cos 3\varphi)\rho_\varepsilon + \frac{1}{2}K_\varepsilon\rho_\varepsilon^{\,2} \quad (A2)$$

Via the minimization of E_- in eqA1, with respect to ρ_ε, one obtains, as the radial distortion parameter,

$$\rho_\varepsilon^{\,m} = \frac{A_1}{K_\varepsilon - 2A_2\cos 3\varphi} \quad (A3)$$

which is defined using the deviations of the bond lengths Δa_i ($i = x, y, z$) from those in the regular reference octahedron:

$$\rho_\varepsilon = \left\{2(\Delta a_x^{\,2} + \Delta a_y^{\,2} + \Delta a_z^{\,2})\right\}^{1/2} \quad (A4)$$

The ground-state stabilization energy is

$$E_-^{\,m} = \frac{-(1/2)A_1^{\,2}}{K_\varepsilon - 2A_2\cos 3\varphi} \equiv -E_{JT} \quad (A5)$$

The angular parameter φ is related to the Δa_i values via

$$\varphi = \arctan\sqrt{3}\left(\frac{(\Delta a_x - \Delta a_y)}{2\Delta a_z - \Delta a_x - \Delta a_y}\right) \quad (A6)$$

As may be deduced from eqA5, the absolute minima in the ground-state potential surface appear at the positions $\varphi_m = 0°$, 120°, and 240°, which specify tetragonally elongated octahedra with the energy given as

$$E_{JT} = \frac{1}{2}\left(\frac{A_1^{\,2}}{K_\varepsilon - 2A_2}\right) \quad (A7)$$

while the saddlepoints at $\varphi_m = 60°$, 180°, and 300° define D_{4h}-compressed octahedra. The energy expression for the Franck–Condon transition within the ^2E_g ground state (see Figure 2), for an arbitrary φ-value, is easily derived from eq A2:

$$E_{FC} = 2\{A_1 + A_2\rho_\varepsilon^{\,m}\cos 3\varphi\}\rho_\varepsilon^{\,m} \quad (A8)$$

The vibronic interaction, discussed here, is formally a pseudo-JT-problem of—in one electron nomenclature—$(e_g + a_{1g}) \otimes \varepsilon_g$ nature, if one includes the excited a_{1g} (4s)-MO into the basis set of wave-functions. There is overwhelming experimental evidence, however (see the main text), that the $e_g \otimes \varepsilon_g$ coupling, by far, dominates the vibronic energy in cases of small to moderate JT-distortions, as present in the treated fluoride solids. Accordingly, the a_{1g} $(3d_z^{\,2})$–a_{1g} (4s) interaction is considered as a higher-order perturbation, with respect to A_1 and included into the vibronic constant A_2.

APPENDIX B

The Inclusion of Strain

Accounting for the binding strain increments, with contributions $+(-)A_1^{\,s}\rho_\varepsilon\cos\varphi_s$ supplementing the diagonal positions at $d_z^{\,2}$ $(d_{x^2-y^2})$ in the basic matrix (1), and with $(-A_1^{\,s}\rho_\varepsilon\sin\varphi_s)$ additions to the non-diagonal positions, the energy eq A1 has now the form:

$$E_{+/-} = \pm\{A_1^{\,2} + 2A_1^{\,s}A_1\cos(\varphi - \varphi_s) + 2A_1A_2\rho_\varepsilon\cos 3\varphi + 2A_1^{\,s}A_2\rho_\varepsilon\cos(2\varphi + \varphi_s) + A_1^{\,s2} + A_2^{\,2}\rho_\varepsilon^{\,2}\}^{1/2} + f(K) \quad (B1)$$

or simplified, for $A_1^{\,s2}$, $A_2^{\,2}\rho_\varepsilon^{\,2} \ll A_1^{\,2}$:

$$E_{+/-} = \pm\{A_1 + A_1^{\,s}\cos(\varphi - \varphi_s) + A_2\rho_\varepsilon\cos 3\varphi\}\rho_\varepsilon + f(K) \quad (B2)$$

The restoring energy additions to the diagonal energies of the matrix given in eq 1 are as follows, if the elastic strain perturbations via K_s (φ_s') and K_{co} $(\varphi_s'' = 90°)$ are included:

$$f(K) = \frac{1}{2}\{K_\varepsilon - K_s\cos(\varphi - \varphi_s') + K_{co}\cos 2\varphi\}\rho_\varepsilon^{\,2} \quad (B3)$$

The minimization of the energy expressions described by eqs B2 and B3, with respect to ρ_ε, yields

$$\rho_\varepsilon^{\,m} = \frac{A_1 + A_1^{\,s}\cos(\varphi - \varphi_s)}{K_\varepsilon - K_s\cos(\varphi - \varphi_s') + K_{co}\cos 2\varphi - 2A_2\cos 3\varphi} \quad (B4)$$

$$E_-^{\,m} = -E_{JT} = -\frac{1}{2}(A_1 + A_1^{\,s}\cos(\varphi - \varphi_s))\rho_\varepsilon^{\,m} \quad (B5)$$

Finally, one obtains, from the minimization of E_{JT}, with respect to the angular parameter, the following condition for φ_m:

$$-2A_1^{\,s}\sin(\varphi_m - \varphi_s) = \{6A_2(4\cos^2\varphi_m - 1)\sin\varphi_m + K_s\sin(\varphi_m - \varphi_s') - 4K_{co}\cos\varphi_m\sin\varphi_m\}\rho_\varepsilon^{\,m} \quad (B6a)$$

or, with $\varphi_s = \varphi_s' = 180°$ and after division by $\sin\varphi_m$, which implies the solutions $\varphi_m = 0°$, 180°:

$$2A_1^{\,s} = \{6A_2(4\cos^2\varphi_m - 1) - K_s - 4K_{co}\cos\varphi_m\}\rho_\varepsilon^{\,m} \quad (B6b)$$

If $A_1^{\,s}$ is of vanishing magnitude, eq B6b further simplifies:

$$\cos^2\varphi_m - \left(\frac{K_{co}}{6A_2}\right)\cos\varphi_m = 0.25\left(1 + \frac{K_s}{6A_2}\right) \quad (B6c)$$

The ground-state splitting emerges as

$$E_{FC} = 2\{A_1 + A_1^{\,s}\cos(\varphi_m - \varphi_s) + A_2\rho_\varepsilon^{\,m}\cos 3\varphi_m\}\rho_\varepsilon^{\,m} \quad (B7)$$

dx.doi.org/10.1021/ic202209c | Inorg. Chem. 2012, 51, 4458–4472

APPENDIX C

Optical Spectroscopy

If one assigns the d−d bands of mixed crystals of $Ba_2Zn_{1-x}Cu_xF_6$,[5] $K_2Zn_{1-x}Cu_xF_4$,[8,16] and $KZn_{1-x}Cu_xF_3$[16,17] in the energy range between 5 and 15 × 10^3 cm^{-1}, according to the A_g [B_{1g} or A_{1g}] → A_g [A_{1g} or B_{1g}], → B_{1g} [B_{2g}] and → B_{2g}, B_{3g} [E_g] transitions in D_{2h} [D_{4h}, elongated or compressed] symmetry, the consistent quantitative analysis demands, when implying a common Δ-parameter of 6.8 (2) × 10^3 cm^{-1}, molecular structures with $D_{4h}{}^e$ symmetries or with D_{2h} symmetries rather near to D_{4h}-elongated (φ_m = 120°, 240°) in most cases. In Ba_2CuF_6[5] and $K_2Zn(Cu)F_4$,[16] however, the octahedra embody distortions close to intermediate between $D_{4h}{}^e$ and $D_{4h}{}^c$, while they are tetragonally compressed in the barium mixed crystals at low *x*-values[42] (see Table 1). One generally must consider, if one compares *structural* results (from diffraction methods) with *bond-strength* results (accessible from optical spectroscopy, for example) that these two properties do not necessarily match *quantitatively* (see Tables 1 and 2). It is deduced from the experiment that the Zn−F_t bonds are slightly shorter than the Zn−F_b bonds, in K_2ZnF_4 and, in particular, in Ba_2ZnF_6, although the bond strength does not differ noticeably ($A_1{}^s$ is close to zero in the copper compounds). Accordingly, the apparent bond-length anisotropy between the shorter Cu−F_b and the Cu−F_t spacings in the JT-distorted octahedra is (slightly) different from the one mirrored by the bond strength, with the latter generating larger φ_m angles. Accordingly, the bond-strength-based molecular distortions (Table 2) are closer to $D_{4h}{}^e$ than the structural data in Table 1 indicate, in the case of K_2CuF_4, and farther away from $D_{4h}{}^e$, if Ba_2CuF_6 is inspected. Also here, we meet the ubiquitous problem—to repeat the essential—that *bond length and bond strength do not necessarily very closely follow each other*, even when the same ligand is considered and only the higher-sphere environment of the ligator atoms differs.

From the observed splittings of the excited T_{2g} states (presuming a near-to-D_{4h} molecular symmetry), the respective $T_{2g} \otimes \varepsilon_g$ coupling parameter is accessible via the expression

$$3\delta_2 = \frac{3}{2} V_\varepsilon \rho_\varepsilon{}^m \tag{C1}$$

where $\rho_\varepsilon{}^m$ refers to the ground-state radial distortion. Again, as for A_1, it is assumed that the coupling constant V_ε is isotropic within the CuF_6 octahedron. In coarse estimation, V_ε is derived to be ∼0.56(5) eV $Å^{-1}$ from the data in Tables 1 and 2, and these are accordingly considerably smaller (by a factor of ∼2) than A_1, as expected for an only π-antibonding electronic state.

EPR Spectroscopy

The g_z component of the *g*-tensor for octahedral Cu^{2+}, as given by perturbation theory, is of the magnitude[11,43]

$$\begin{aligned} g_z = g_o + 4u_z - 2(u_x{}^2 + u_y{}^2) - (u_x u_z - u_x u_y + u_y u_z) \\ + \{4u_z + (u_x{}^2 + u_y{}^2) - (u_{xz} + 2u_x u_y + u_y u_z)\} \\ \cos\varphi + \{(u_y{}^2 - u_x{}^2) - (u_{xz} - u_{yz})\}\sqrt{3}\ \sin\varphi \end{aligned} \tag{C2}$$

where *z* is the direction parallel to the M^{II}−F_t bond (see Figure 2). Equation C1 simplifies to

$$g_\parallel = g_0 - 3u_\perp{}^2 \qquad g_\perp = g_0 + 6u_\perp - 6u_\perp{}^2 \tag{C3a}$$

for φ = 180° and

$$g_\parallel = g_0 + 8u_\parallel - 4u_\parallel u_\perp - 3u_\perp{}^2$$
$$g_\perp = g_0 + 2u_\perp - 4u_\parallel{}^2 \tag{C3b}$$

for φ = 0°.

The orbital contributions u_i (for $i = z, x, y$) are defined as

$$u_i = k^2\left(\frac{\lambda_0}{E_i}\right) \tag{C3c}$$

k ($\cong k_x \cong k_y \cong k_z$) is the covalency factor and is experimentally found to be 0.85 for Ba_2CuF_6 and K_2CuF_4; λ_0 is the free-ion spin-orbit coupling parameter for Cu^{2+} (λ_0 = 830 cm^{-1}), and the E_i term represents the d−d transition energies to $B_{1g}(z)$, $B_{2g}(x)$, and $B_{3g}(y)$, respectively (see Figure 2). If, for example, two D_{4h}-elongated conformations at φ = 120° and 240° would dynamically equilibrate via a low energy barrier at φ = 180°, the following *g*-tensor components are derived:

$$\begin{aligned} g_\parallel(\mathrm{dyn}) &= g_\perp \\ &= g_0 + 2u_\perp - 4u_\parallel{}^2 \\ &\cong g_0 + 2u - 4u^2 \end{aligned} \tag{C4a}$$

$$\begin{aligned} g_\perp(\mathrm{dyn}) &= \frac{1}{2}(g_\parallel + g_\perp) \\ &= g_0 + 4u_\parallel + u_\perp - 2u_\parallel{}^2 - 2u_\parallel u_\perp - 1.5u_\perp{}^2 \\ &\cong g_0 + 5u - 5.5u_\perp{}^2 \end{aligned} \tag{C4b}$$

These are substantially different from those in eqC3a, although the EPR spectrum has the symmetry appearance according to a tetragonal compression with $g_\parallel < g_\perp$. Obviously, EPR has the potential, via the magnitudes of the orbital contributions, to sensibly distinguish a static distortion from a situation, where partial or complete dynamic averaging occurs. The octahedron distortion in the mixed-crystal series $Ba_2Zn_{1-x}Cu_xF_6$[5] and $K_2Zn_{1-x}Cu_xF_4$[8] has been analyzed, mainly using such types of arguments.

The $g_\parallel$-tensor component for Cu^{2+}-doped Ba_2ZnF_6 is calculated to be 1.99_0, when utilizing the energies in Table 2; this is in perfect agreement with the experiment and, hence, with a pure d_{z^2} ground state. However, the $g_\parallel$-tensor component increases slightly by 0.01_4, when increasing the temperature from 4.2 K to 300 K—thus suggesting a small admixture of orbital contributions from $g_\parallel$ (0°) to $g_\parallel$ (180°) (see eqs C3a and C3b); the obvious reason is the population of higher vibrational levels (here not considered) in the broad minimum of the ground state potential curve (see Figure 8).

The EPR spectra of Cu^{2+}-doped K_2ZnF_4 also demand a D_{4h}-compressed molecular geometry of the doped centers at first sight, which virtually contrasts with the results from d−d spectroscopy (see Table 2). However, the $g_\parallel$-value at 4.2 K (2.00_3) is $\sim 0.01_5$ larger than expected for a pure d_{z^2} ground state at φ = 180°, suggesting dynamic equilibration effects as already considered in eqs C4 at this temperature. More explicitly, the latter deviation originates from the zero-point

dx.doi.org/10.1021/ic202209c | Inorg. Chem. 2012, 51, 4458−4472

mean square angular vibration, with an amplitude $\langle\alpha^2\rangle_0$, where $\alpha = \varphi - 180°$. In this dynamic approach, $g_{\|}$ is of the form

$$g_{\|} = g_{\|}(d_{z^2})\left\langle \cos^2\left(\frac{a}{2}\right)\right\rangle + g_{\|}(d_{x^2-y^2})\left\langle \sin^2\left(\frac{a}{2}\right)\right\rangle \quad \text{(C5)}$$

yielding an angular delocalization of roughly 180° ± 20°, when utilizing $u_{\perp}$ (180°) ≅ 0.07_0 and $u_{\|}$ (0°) ≈ 0.07_S, as derived from the information in Tables 1 and 2 and eqs C3. The further increase of $g_{\|}$ by ≅0.04 when increasing the temperature to 300 K is considerably larger than that observed in the Ba_2ZnF_6 (Cu^{2+}) case; this observation matches the comparatively much broader shape of the potential energy surface, which, when inspecting the curve at an excitation energy of 0.02_S eV (≈ 300 K), stretches over a range of $\delta\varphi \approx 260°$, in comparison to Cu^{2+} in the Ba_2ZnF_6 host with 140° (see Figure 8). In addition to the more-pronounced delocalization, a significant partial occupation of the upper minimum at $\varphi_m = 0$ is expected to occur.

Usually, one does not observe the EPR spectra of the single-molecular Cu^{2+} octahedra in the cases of mixed crystals with a high copper concentration. Exchange interactions between two differently oriented (near to) D_{4h}^{e}-distorted octahedra in the planes ⊥c (see Figure 5)—and, hence, between the two sublattices at $\varphi \approx 120°$ and 240°, which constitute the antiferrodistortive order (see Figure 6)—may lead to an averaging of the g_x (≅ $g_{\|}$ or $g_{\perp}$)- and g_y (≅ $g_{\perp}$ or $g_{\|}$)-tensor components in that plane (see Figure 7), giving the resulting spectrum the symmetry appearance expected for a tetragonally compressed species[44] (index "ex" refers to exchange-coupled), although the orbital contributions distinctly differ from those in eq C3a. The respective analytical expressions for $g_{\|}^{ex}$ and $g_{\perp}^{ex}$ are analogous to those in the case of dynamic averaging (eqs C4).

■ ASSOCIATED CONTENT

Related Articles

†A short version of this article was presented at the 20th International Symposium on the Jahn–Teller Effect in Fribourg, Switzerland, August 2010.

■ AUTHOR INFORMATION

Notes

The authors declare no competing financial interest.

■ ACKNOWLEDGMENTS

The author appreciates the friendly support of Prof. W. Petz (Marburg) in transforming in particular the figures into a publication-ready form.

■ REFERENCES

(1) Pearson, R. G. *Symmetry Rules for Chemical Reactions: Orbital Topology and Elementary Processes*; Wiley–Interscience: New York, 1976 (in particular, see: Application of Perturbation Theory).
(2) Reinen, D.; Atanasov, M. *Magn. Reson. Rev.* **1991**, *15*, 167–239.
(3) Figgis, B. N.; Hitchman, M. *Ligand Field Theory and its Applications*; Wiley–VCH: Weinheim, Germany, 2000.
(4) (a) Herdtweck, E.; Babel, D. *Z. Kristallogr.* **1980**, *153*, 189. (b) von Schnering, H. G. *Z. Anorg. Allg. Chem.* **1967**, *353*, 13–25.
(5) Friebel, C.; Propach, V.; Reinen, D. *Z. Naturforsch.* **1976**, *31b*, 1574–1584.
(6) (a) Krause, S. Diploma Thesis, Fachbereich Chemie der Philipps-Universität, Marburg, Germany, 1976. (b) Steffens, F. Doctoral Thesis, Fachbereich Chemie der Philipps-Universität, Marburg, Germany, 1978.
(7) Friebel, C. *Z. Naturforsch.* **1974**, *29b*, 634–641. Reinen, D.; Weitzel, H. *Z. Naturforsch.* **1977**, *32b*, 476–478.
(8) Reinen, D.; Krause, S. *Inorg. Chem.* **1981**, *20*, 2750–2759 and references cited therein.
(9) Okazaki, O.; Suemune, Y. *J. Phys. Soc. Jpn.*, **1961**, *16*, 176–182 and 671–675.
(10) Propach, V.; Steffens, F. *Z. Naturforsch.* **1978**, *33b*, 268–274.
(11) Reinen, D.; Friebel, C. *Structure and Bonding 37*; Springer: Berlin, New York, 1979; pp 1–60 and references cited therein.
(12) Ham, F. S. Jahn–Teller Effects in Electron Paramagnetic Resonance Spectra. In *Electron Paramagnetic Resonance*; Plenum Press, New York, 1972 (and *Phys. Rev.* **1965**, *A138*, 1727).
(13) Reinen, D.; Atanasov, M.; Köhler, P.; Babel, D. *Coord. Chem. Rev.* **2010**, *254*, 2703–2754.
(14) Bacci, M.et al. *Chem. Phys. Lett.*, **1978**, *58*, 537 and *Chem. Phys.* **1979**, *40*, 237.
(15) Riley, M. J.; Dubicki, L.; Moran, G.; Krausz, E. R.; Yamada, I. *Inorg. Chem.* **1990**, *29*, 1614–1626.
(16) Dubicki, L.; Krausz, E.; Riley, M. J.; Yamada, I. *Chem. Phys. Lett.* **1989**, *157*, 315–320.
(17) Friebel, C.; Reinen, D. *Z. Anorg. Allg. Chem.* **1974**, *407*, 193–200.
(18) Friebel, C.; Pebler, J.; Steffens, F.; Weber, M.; Reinen, D. *J. Solid State Chem.* **1983**, *46*, 253–264.
(19) Duffy, J. A. *Bonding, Energy Levels and Bands in Inorganic Solids*; Longman/Wiley: New York, 1990; Chapter 6.
(20) Jorgensen, C. K. *Oxidation Numbers and Oxidation States*; Springer: Berlin, New York, 1969 and *Structure and Bonding 3*; Springer–Verlag: Berlin, New York, 1966; pp 106–115.
(21) Reinen, D.; Atanasov, M.; Lee, S.-L. *Coord. Chem. Rev.* **1998**, *175*, 91–158.
(22) Steffen, G.; Reinen, D.; Stratemeier, H.; Riley, M. J.; Hitchman, M.; Matthies, H. E.; Recker, K.; Wallrafen, F.; Niklas, J. R. *Inorg. Chem.* **1990**, *29*, 2123–2131.
(23) (a) Anikeenok, O. A.; Gumerov, R. M.; Eremin, M. V.; Ivanova, T. A.; Yablokov, Yu. V. *Sov. Phys. Solid State* **1984**, *26*, 1365. (b) Eremin, M. V.; Yablokov, Yu. V.; Ivanova, T. A.; Gumerov, R. M. *Sov. Phys. JETP* **1984**, *60*, 128.
(24) (a) Hitchman, M. A.; McDonald, R. G.; Reinen, D. *Inorg. Chem.* **1986**, *25*, 519–522. (b) Riley, M. J.; Hitchman, M. A.; Reinen, D. *Chem. Phys.* **1986**, *102*, 11–28.
(25) Kaplan, M. D.; Vekhter, B. G. *Cooperative Phenomena in Jahn–Teller Systems*; Plenum Press: New York, 1995.
(26) (a) Steffens, F.; Reinen, D. *Z. Naturforsch.* **1976**, *31b*, 894–896. (b) Reinen, D.; Steffens, F. *Z. Anorg. Allg. Chem.* **1978**, *441*, 63–82.
(27) (a) Köhl, P.; Reinen, D.; Decher, G.; Wanklyn, B. *Z. Kristallogr.* **1980**, *153*, 211–220. (b) Mayer, H. W.; Reinen, D.; Heger, G. *J. Solid State Chem.* **1983**, *50*, 213–224.
(28) Bersuker, I. B. *The Jahn–Teller Effect*; Cambridge University Press: Cambridge, U.K., 2006; Section 8.1.2 and references cited therein.
(29) Gazo, J.; Bersuker, I. B.; Garaj, J.; Kabesova, M.; Kohout, J.; Langfelderova, H.; Melnik, M.; Serator, M.; Valach, F. *Coord. Chem. Rev.* **1976**, *19*, 253–297.
(30) Atanasov, M.; Hitchman, M. A.; Hoppe, R.; Murray, K. S.; Moubaraki, B.; Reinen, D.; Stratemeier, H. *Inorg. Chem.* **1993**, *32*, 3397–3401.
(31) Riley, M. J.; Hitchman, M. A.; Wan Mohammed, A. J. *J. Chem. Phys.* **1987**, *87*, 3766–3778.
(32) (a) Riley, M. J.; Hitchman, M. A.; Reinen, D. *Chem. Phys.* **1986**, *102*, 11–28. (b) Simmons, C. J.; Stratemeier, H.; Hitchman, M. A.; Reinen, D.; Masters, V. M.; Riley, M. J. *Inorg. Chem.* **2011**, *50*, 4900–4916 (DOI: 10.1021/ic200554f).
(33) (a) Grande, B.; Müller-Buschbaum, Hk. *Z. Anorg. Allg. Chem.* **1974**, *433*, 152–156. (b) Grande, B.; Müller-Buschbaum, Hk.; Schweizer, M. *Z. Anorg. Allg. Chem.* **1977**, *428*, 120–124.
(34) Reinen, D.; Wegwerth, J. *Physica C* **1991**, *183*, 261–276.
(35) Bednorz, J. G.; Müller, K. A. *Z. Phys. B* **1986**, *64*, 189.

(36) Reinen, D.; Atanasov, M. In *The Jahn−Teller Effect: Fundamentals and Implications for Physics and Chemistry*; Köppel, H., Yarkony, D. R., Barentzen, H., Eds.; Springer Series in Chemistry and Physics; Springer: Heidelberg, New York, 2009; Vol. *97*, p 451.
(37) Abou-Warda, S.; Pietzuch, W.; Berghöfer, G.; Kesper, U.; Massa, W.; Reinen, D. *J. Solid State Chem.* **1998**, *138*, 18−31.
(38) Garcia-Lastra, J. M.; Aramburu, J. A.; Barriuso, M. T.; Moreno, M. *Chem. Phys. Lett.* **2004**, *385*, 286−291.
(39) Ziegler, T. In *Molecular Electronic Structures of Transition Metal Complexes; Structure Bonding* 143; Springer: Berlin, New York, 2011; Sections 1−3.2. Atanasov, M.; Ganiyushin, D.; Sivalingam, K.; Neese, F. In *Structure Bonding* 142, 2011; Sections 1−6.1. (Both volumes in honorary for C.J. Ballhausen.)
(40) Delley, B. *J. Chem. Phys.* **2000**, *113*, 7756.
(41) *Optical Spectra and Chemical Bonding in Inorganic Compounds*; Structure and Bonding 106; Springer: Berlin, New York, 2004. (Honorary for C. K. Jorgensen.)
(42) Reinen, D.; Steffen, G.; Hitchman, M. A.; Stratemeier, H.; Dubicki, L.; Krausz, E. R.; Riley, M. J.; Mathies, H. E.; Recker, K.; Wallrafen, F. *Chem. Phys.* **1991**, *155*, 117−125.
(43) McGarvey, B. R. ESR of Transition Metal Complexes. In *Transition Metal Chemistry*; Marcel Dekker: New York, 1966; Vol. *3*, pp 88−199.
(44) (a) Reinen, D. *Solid State Commun.* **1977**, *21*, 137−140. (b) Reinen, D.; Dance, J.-M. Local and Cooperative Effects in the EPR Spectra of Transition Metal Fluorides. In *Inorganic Solid Fluorides*; Academic Press: New York, 1985; pp 525−543.

■ NOTE ADDED AFTER ASAP PUBLICATION

Equation 6 contained errors and a reference citation in the Table 1 footnote was incorrect in the version published ASAP March 14, 2012. The correct version reposted March 23, 2012.